


**Statistical moments of the interspike intervals for a neuron model driven by trichotomous noise**Romi Mankin, Astrid Rekker \*, and Sander Paekivi*School of Natural Sciences and Health, Tallinn University, 29 Narva Road, 10120 Tallinn, Estonia*

(Received 2 February 2021; accepted 14 May 2021; published 1 June 2021)

The influence of a colored three-level input noise (trichotomous noise) on the spike generation of a perfect integrate-and-fire (PIF) model of neurons is studied. Using a first-passage-time formulation, exact expressions for the Laplace transform of the output interspike interval (ISI) density and for the statistical moments of the ISIs (such as the coefficient of variation, the skewness, the serial correlation coefficient, and the Fano factor) are derived. To model the anomalous subdiffusion that can arise from, e.g., the trapping properties of dendritic spines, the model is extended by including a random operational time in the form of an inverse strictly increasing Lévy-type subordinator, and exact formulas for ISI statistics are given for this case as well. Particularly, it is shown that at some parameter regimes, the ISI density exhibits a three-modal structure. The results for the extended model show that the ISI serial correlation coefficient and the Fano factor are nonmonotonic with respect to the input current, which indicates that at an intermediate value of the input current the variability of the output spike trains is minimal. Similarities and differences between the behavior of the presented models and the previously investigated PIF models driven by dichotomous noise are also discussed.

DOI: [10.1103/PhysRevE.103.062201](https://doi.org/10.1103/PhysRevE.103.062201)**I. INTRODUCTION**

Stochastic fluctuations often evoke an unexpected response in physical, chemical, and biological systems; the response may consist in stochastic resonance [1–3], the ratchet effect [4,5], hypersensitive transport [6,7], and anomalous diffusion [8–12], to name a few. Especially during the past decades, noise-dependent behavior of neural systems has received considerable attention. As the dynamics of a neuron's electrical activity is quite complex, reduced models capturing the fundamental features of this process in mathematically simpler terms are of interest in neuroscientific applications [13–25]. Moreover, an understanding of neuronal mechanisms gained from reduced models could be useful in the engineering of artificial neural devices designed to reproduce a given real biological feature [21]. The simplest example of such a reduced model is the white noise driven perfect integrate-and-fire (PIF) model [14]. For the first time it was obtained by modeling the neuron's membrane potential evolution as a common random walk [13]. However, research suggests that the effect of synaptic inputs on the dynamics of the neuron's membrane potential cannot always be characterized by white noise, but rather by a stochastic process with a finite amplitude and correlation time (i.e., by a colored noise), which does not have Gaussian statistics [25–28]. Most of the analytical results for the cases of input colored noises have been obtained in the limits of slow and fast noises [29], as well as in a weak noise approximation [18,24]. Exceptions are integrate-and-fire (IF) models with a synaptic input described by dichotomous noise [30], which can give analytically tractable exact results [26,29,31–33]. The analytical

results achieved in these papers demonstrate a set of important features of the interspike interval (ISI) distribution that stem from noise correlation. Particularly, in contrast to the PIF model with Gaussian input, the ISI distribution is clearly bimodal for small transition rates of the input dichotomous noise.

It is empirically known that the ISI density of real neurons (e.g., pallidal and ganglion cells) can exhibit nontrivial patterns, such as a bimodal or multimodal structure depending on the input [21,34–36]. We would note that the conventional models [14] driven by Gaussian noise are not able to produce such a multimodal structure [21]. Thus, it is of interest, from both theoretical and possible experimental viewpoints, to know the behavior of the output ISI statistics of a PIF model subjected to a colored three-level Markovian noise (called trichotomous noise [3,7]). Especially, to find an answer to the question whether the input trichotomous noise in the PIF model can cause a three-modal structure of the output ISI distribution. In the neurobiological context, trichotomous noise is particularly suitable to mimic three-level state inputs which may arise from presynaptic randomly bursting neural populations [37,38]. Of course, such a model is a gross oversimplification of any natural neuron. The usual IF models consider the neuron to be a single compartment that receives inputs from dendrites, whose morphology and effects related to the latter are disregarded. Moreover, empirical investigations show that some neocortical neurons operate as fractional differentiators [39], which indicate possible power-law distributed waiting times between the excitatory (or inhibitory) synaptic inputs. Recently, the authors of Refs. [40,41] attempted to phenomenologically include these effects by describing the effective input of IF models by a subordinated process (i.e., by introducing a random operational time).

\*astrid.rekker@tlu.ee

In this paper, inspired by results of [26,41] and by the reasons presented above, we consider a stochastic PIF model driven by a trichotomous noise. An extension of this model to a more elaborate subordinated model with a random operational time in the form of an inverse strictly increasing Lévy-type subordinator [41] is also investigated. The aim of the paper is to demonstrate that aside from the dichotomous noise the trichotomous noise input is another example of a driving non-Gaussian colored noise that can lead to exact results for PIF neurons. We provide an exact analytical formula for the Laplace transform of the output ISI density. On the basis of this formula we have derived exact expressions for the dependence of statistical characteristics of the output spike train, such as the average ISI, the variance, the skewness, the serial correlation coefficient (SCC), and the Fano factor, on the input parameters.

Particularly, it is shown that both models (with and without subordination) predict at some parameter regimes a three-modal output ISI distribution. Moreover, for the case with subordination the SCC demonstrates a nonmonotonic dependence on the mean input current  $\mu$ , which indicates that the ISI regularity is maximized at this value of  $\mu$ . The latter effect was previously reported in Ref. [41] for a subordinated PIF model driven by a dichotomous noise. This behavior of the SCC is in sharp contrast with the behavior of the SCC without subordination. In the latter case the SCC always increases monotonically to 1 when  $\mu$  increases.

The structure of the paper is as follows. In Sec. II, we present the model investigated. In Sec. III, exact formulas are found for the Laplace transform of the ISI density. In Sec. IV, exact formulas are derived for the ISI statistics. In Sec. V, we discuss the behavior of the statistical measures and illustrate their characteristic features. Section VI contains some brief concluding remarks. Some formulas are delegated to the Appendices.

## II. MODEL

In neuroscientific applications, one of the most used reduced neuron models is the IF model, which describes, neglecting the morphology of dendrites, the dynamics of the neuron's membrane potential in terms of synaptic inputs and injected current [14,15]. This model describes the dynamics of the membrane potential in time as a solution of a differential equation, supplemented by a spike generation rule, which states that a spike is considered to have occurred once the potential reaches a fixed threshold value, and is reset to an initial value after that. The simplest but widely accepted as one of the canonical models in this class is the PIF model, which features a linear input current and a threshold at spike onset. The PIF model is a good approximation for some complicated neural models if the mean input current is large [13,42].

### A. Ordinary PIF model driven by trichotomous noise

Our starting point is an archetypical stochastic PIF model of subthreshold dynamics, written as in [13,31]

$$\frac{d}{dt}V(t) = \mu + Z(t), \quad (1)$$

where  $V(t)$  is the membrane potential at time  $t$  measured in the units of the membrane time constant  $\tau_m$ ,  $\tau_m = 1$ ;  $\mu > 0$  is a constant proportional to the average input current if synaptic inputs are considered homogeneous, and  $Z(t)$  is the fluctuating part of an input current. In Eq. (1),  $Z(t)$  is to be assumed as a trichotomous noise [3,7]. The trichotomous noise is a random stationary Markovian process that consists of jumps between three values:  $z_1 = a$ ,  $z_2 = 0$ , and  $z_3 = -a$ . The jumps follow in time a Poisson process, while the values  $z_1$ ,  $z_3$ , and  $z_2$  occur with the stationary probabilities

$$p_1 = p_3 = q, \quad p_2 = 1 - 2q, \quad (2)$$

with  $0 < q \leq \frac{1}{2}$ . The mean value and the correlation function are

$$\langle Z(t) \rangle = 0, \quad \langle Z(t)Z(t') \rangle = 2qa^2 e^{-\nu|t-t'|}. \quad (3)$$

It can be seen that the switching rate  $\nu$  is the reciprocal of the noise correlation time  $\tau_c$ , i.e.,  $\tau_c = 1/\nu$ . More details on the trichotomous process can be found in Appendix A. Although both dichotomous and trichotomous noises may be useful in modeling natural colored fluctuations, the latter is more flexible, including also the case of dichotomous noise ( $q = \frac{1}{2}$ ). Particularly, for trichotomous noises, the kurtosis  $\kappa$  can be anything from  $-2$  to  $\infty$ , unlike the kurtosis for Gaussian colored noise,  $\kappa = 0$ , and symmetric dichotomous noise,  $\kappa = -2$ . This extra degree of freedom can prove useful in modeling actual fluctuations. Moreover, the trichotomous noise  $Z(t)$  can be represented as the sum of two cross-correlated zero-mean symmetric dichotomous noises  $Z_1(t)$  and  $Z_2(t)$ , i.e.,

$$Z(t) = Z_1(t) + Z_2(t). \quad (4)$$

The dichotomous noises  $Z_1(t)$  and  $Z_2(t)$  are characterized as follows [3]:  $Z_1, Z_2 \in \{(\frac{1}{2})a, -(\frac{1}{2})a\}$  with  $\nu_1 = \nu_2 = \nu$  and the correlation function

$$\langle Z_i(t)Z_j(t') \rangle = \rho_{ij} \frac{a^2}{4} e^{-\nu|t-t'|}, \quad i, j = 1, 2 \quad (5)$$

where  $\rho_{ii} = 1$  and  $\rho_{ij} = \rho = 4q - 1 \in (-1, 1)$  with  $i \neq j$  being the cross-correlation intensity of the noises  $Z_1(t)$  and  $Z_2(t)$ . As a dichotomous noise is suitable to mimic the up-down state inputs of a neuron receiving input from a randomly bursting neural population [25,26,37,38,43], in the biophysical context a trichotomous noise may be considered as an approximation of the synaptic inputs arriving in the soma of a neuron via dendrites from two partially correlated randomly bursting neural populations.

Model (1) is supplemented by the spike generator rule: if the voltage reaches a certain threshold value  $V(t) = v_c$ , then a spike is considered to have occurred at time  $t$  and the voltage is reset to zero. In the following, we assume that the spike generating process is a stationary process and limit the analysis to the case in which

$$\mu \pm a > 0. \quad (6)$$

This condition implies that the voltage passes the threshold in all states of the trichotomous noise. In the case of  $q = \frac{1}{2}$ , model (1) reduces to the PIF model driven by a dichotomous noise previously considered in [31].

### B. Subordination method

Over the last decades it has become apparent that many complex systems exhibit anomalous subdiffusion with a mean-square displacement of particles  $\langle r^2(t) \rangle \sim t^\alpha$  ( $\alpha < 1$ ) [8]. For a description of relaxation and transport properties in such systems the continuous-time random walk (CTRW) process is one of the most useful mathematical tools [9,44–49]. This process generalizes the standard random walk and allows for random waiting times between jumps of random length. In the decoupled case the CTRW is characterized by a waiting time distribution and an independent jump length distribution. The power-law behavior of the mean-square displacement corresponds to a CTRW model in which the interjump times obey a distribution density with the characteristic power tail  $\Psi(t) \sim t^{-(1+\alpha)}$  for large  $t$ ,  $0 < \alpha < 1$ . The parameter  $\alpha$  has its origin in a random activation energy scenario, where a particle is trapped in a given configuration of microscopic potential barrier heights which give rise to a hierarchy of waiting times [49]. In the diffusion limit (a continuous realization of the CTRW) such systems can be modeled by the use of the subordination method [44,45], which is described by a system of coupled Langevin equations [44]

$$\frac{d}{dt}X(\tau) = F(X(\tau)) + \xi(\tau), \quad \frac{d}{d\tau}T(\tau) = \eta(\tau), \quad (7)$$

where  $F(x)$  is a time independent external force; the trajectories  $y(t) = x(\tau(t))$  of the random walk become parametrized by a variable  $\tau$  and the Markovian noises  $\xi(\tau)$  and  $\eta(\tau)$  are assumed to be independent. Here and in the following we denote a stochastic variable with the capital letter (e.g.,  $T$ ) and a possible value of this variable with the corresponding lower case letter (e.g.,  $t$ ). In this context,  $\eta(\tau)$  has to be positive due to causality.

In Eqs. (7) the parameter  $\tau$  (internal time) plays the role of the number of jumps performed along the trajectory  $x(\tau)$ , and is successively delayed by trapping events, while physical time  $t$  is modeled by an independent random process  $T(\tau)$  called the subordinator. In fact, the subordinator  $T(\tau)$  is nothing else, but the sum of independent, identically distributed random waiting time intervals between the jumps of the walker. To complete the subordination procedure, an inverse subordinator  $S(t)$  is introduced, which measures the evolution of the internal time as a random function of laboratory time  $t$ ,

$$S(t) = \inf\{\tau : T(\tau) > t\}. \quad (8)$$

The process of primary interest, i.e., the particle motion as seen by the observer in physical time  $t$ , is now obtained as a combined random function  $Y(t) = X(S(t))$ . The process  $X(\tau)$  is called a parent process, and the resulting process  $Y(t)$  is subordinated to the parent process (sometimes called the subordinated process). To satisfy the requirements for physical time, the subordinator  $T(\tau)$  is defined as a strictly increasing Lévy motion. This process is Markovian with independent time-homogeneous increments, and such that the Laplace transform of the probability density function (PDF)  $p(t, \tau)$  of  $T(\tau)$  is given by

$$\langle e^{-sT(\tau)} \rangle = \int_0^\infty e^{-st} p(t, \tau) dt = e^{-\tau\phi(s)}, \quad (9)$$

where the function  $\phi(s)$  is called the Lévy exponent. If  $\phi(s)$  is a Bernstein function with  $\phi(0) = 0$  [41,46], the subordinator  $T(\tau)$  is well defined. It starts from 0 and is a pure-jump process with strictly increasing sample paths. In this case the inverse subordinator  $S(t)$  has nondecreasing continuous trajectories and can be used as a time arrow [46]. Notice that contrary to  $T(\tau)$  the inverse subordinator is a non-Markovian process. The Laplace transform of the PDF  $h(\tau, t)$  of the inverse subordinator  $S(t)$  is given by [46]

$$\hat{h}(\tau, s) = \int_0^\infty h(\tau, t) e^{-st} dt = \frac{\phi(s)}{s} e^{-\tau\phi(s)}. \quad (10)$$

### C. Subordinated PIF model

There is strong evidence that the voltage trace of some neurons (e.g., pyramidal neurons) can follow multiple timescale dynamics [39,50,51]. Such dynamics can result in power-law type behavior in which the membrane voltage cannot be characterized with conventional PIF models. In Refs. [50,52] fractional-order leaky integrate-and-fire models are proposed to help understand the adapting behavior of cortical neurons [50,51], and also to model the anomalous subdiffusion that arises from the trapping properties of dendritic spines [52]. In fractional models the order of the fractional derivative goes from 0 to 1, indicating the occurrence of subdiffusive dynamics in such models. For example, in [52] the Nerst-Planck equation with fractional order operators is used to model the anomalous subdiffusion that arises from the trapping properties of dendritic spines. This model takes into account random motions of ions with trapping effects due to the geometry of spines as well as the drift of ions due to the electric field of the membrane potential. Recently, in Refs. [40,41] an alternative approach for spike generation of neurons is developed based on a subordination procedure. In these papers it is attempted to phenomenologically include the effects of dendrite morphology, the possible timing delays that the latter may cause, and the possible power-law distributed waiting times between synaptic inputs by means of a Lévy-type subordinator.

Following the argumentation presented in Ref. [41], where a subordinated PIF model driven by a dichotomous noise is considered, we generalize model (1) by introducing a random operational (internal) time  $\tau$  via an inverse subordinator  $S(t)$ . According to the subordination procedure (see also Sec. II B), we suppose that the parent process  $V(\tau)$  for the neuron's membrane evolution in the internal time  $\tau$  is governed by Eq. (1), i.e.,

$$\frac{d}{d\tau}V(\tau) = \mu + Z(\tau). \quad (11)$$

To specify the structure of the Lévy exponent  $\phi(s)$ , which determines the inverse subordinator via Eq. (10), we note that the fractional-order leaky integrate-and-fire models [50–52] can also be considered as subordinated models with a Lévy exponent

$$\phi(s) = \frac{1}{\tau_0} (\tau_0 s)^\alpha, \quad (12)$$

where  $0 < \alpha < 1$  and  $\tau_0 = \tau_m$  is the membrane time constant. Although the stochastic model with the Lévy exponent  $\phi(s) \sim s^\alpha$  is very useful for modeling anomalous diffusion

processes, it has some nonphysical properties, e.g., absence of any finite statistical moments of the subordinator  $T(\tau)$ , which indicates synaptic traps with infinite depth in the neuron model. From the physical perspective it is desirable to have a model that circumvents the infinite-moment difficulty while preserving the subdiffusive behavior for small and moderate times. Moreover, transient anomalous diffusion is found to emerge from a wide range of natural complex processes (see Refs. [8,45]); at small and moderate times the behavior of the system is subdiffusive, but demonstrates normal diffusion at long times. References [45,53] are devoted to just this problem. An appropriate modification of the Lévy exponent that leads to finite moments of all orders is proposed in the form [41,45,53]

$$\phi(s) = \frac{[\tau_0(s + \delta)]^\alpha - (\tau_0\delta)^\alpha}{\tau_0[1 + (\tau_0\delta)^\alpha]}, \quad (13)$$

where  $0 < \alpha < 1$ ,  $\tau_0 = \text{const}$  has the dimension of time, and the parameter  $\delta > 0$  characterizes an exponential truncation of the heavy-tailed distribution  $\Psi(t) \sim e^{-\delta t} t^{-(\alpha+1)}$  of waiting times at  $t \rightarrow \infty$ . In this paper we model the Lévy exponent as [41]

$$\phi(s) = \frac{1}{\tau_0} \left[ \sum_{i=1}^n \frac{\eta_i [1 + (\tau_0\delta_i)^{\alpha_i}]}{[\tau_0(s + \delta_i)^{\alpha_i} - (\tau_0\delta_i)^{\alpha_i}]^{\alpha_i}} \right]^{-1}, \quad (14)$$

where  $0 < \alpha_i \leq 1$ ,  $\tau_0 = \text{const}$ ,  $\delta_i > 0$ , and  $\eta_i \geq 0$  characterizes the relative weight of the  $i$ th summand ( $\sum_{i=1}^n \eta_i = 1$ ). As shown in [41], in the biophysical context, such a Lévy exponent can appear if we describe dendrites as  $n$  independent escape channels acting in parallel [the total number of escape events in the time interval  $(0, t)$  is considered as the inverse subordinator  $S(t)$ ]. In the particular case of one channel ( $n = 1$ ) Eq. (14) reduces to Eq. (13).

The subordinated PIF model (under consideration) is defined by Eqs. (8)–(11), and (14), along with the spike generator rule described above by model (1). The corresponding voltage evolution as seen by the observer in the physical time  $t$  is given by (see also Sec. II B)

$$\tilde{V}(t) = V(S(t)). \quad (15)$$

Finally, we note that the mean  $\langle T(\tau) \rangle$ , the coefficient of variation  $C_{T(\tau)}^2 = \langle [T(\tau) - \langle T(\tau) \rangle]^2 \rangle / \langle T(\tau) \rangle^2$ , and the skewness  $\gamma_{T(\tau)} = \langle [T(\tau) - \langle T(\tau) \rangle]^3 \rangle / \langle [T(\tau) - \langle T(\tau) \rangle]^2 \rangle^{3/2}$  of the subordinator  $T(\tau)$  are given by

$$\langle T(\tau) \rangle = \tau \phi^{(1)}(0), \quad C_{T(\tau)}^2 = -\frac{\phi^{(2)}(0)}{\tau (\phi^{(1)}(0))^2} \quad (16)$$

and

$$\gamma_{T(\tau)} = \frac{\phi^{(3)}(0)}{\sqrt{\tau} (-\phi^{(2)}(0))^{3/2}} \quad (17)$$

with  $\phi^{(n)}(s) = d^n \phi(s) / ds^n$ .

### III. ISI DISTRIBUTION

Usually, the output of a neuron is characterized by the statistics of the sequence of intervals between subsequent spikes. Instances at which the membrane potential reaches the threshold  $v_c$  define the spike times  $t_i$ ,  $i = 1, 2, \dots$ , and

thus a sequence of ISIs  $I_i = t_i - t_{i-1}$  as well as the sum of  $n$  subsequent ISIs

$$T_n = \sum_{i=1}^n I_i, \quad (18)$$

called the  $n$ th-order interval, where obviously  $T_1 = I_1$ . The key quantity to characterize the ISI statistics is the output ISI probability density  $w(t)$ . The ISI distribution  $w(t)$  equals the probability density of the time needed to reach the threshold for the first time after starting at the reset value. To find this density, we start from a statistical description of the voltage  $V(t)$  evolution determined by Eq. (1). The following master equation describes the time-dependent behavior of the probability distribution of the joint Markov process  $\{V(t), Z(t)\}$ :

$$\frac{\partial}{\partial t} P_i(v, t) = -(\mu + z_i) \frac{\partial}{\partial v} P_i(v, t) + v \sum_{j=1}^3 S_{ij} P_j(v, t), \quad (19)$$

where  $i, j = 1, 2, 3$ ,  $P_i(v, t)$  are the probability densities that  $V(t) = v$  and  $Z(t) = z_i$ , respectively, and the transition matrix  $S_{ij}$  is given by Eq. (A3). Because of condition (6) the voltage trajectories  $v(t)$  starting from the reset state [ $V(0) = 0$ ] cannot cross the threshold multiple times, and thus the evolution of the probability density in the presence of an absorbing boundary is the same as that in the absence of such a boundary. Hence, for the stationary spike train the ISI distribution  $w(t)$  is given by the probability current in the  $v$  direction,

$$J(v, t) = \sum_{i=1}^3 (\mu + z_i) P_i(v, t) \quad (20)$$

taken at the absorbing threshold  $V(t) = v_c$ , i.e.,

$$w(t) = J(v_c, t). \quad (21)$$

The transition probability densities  $P_{ij}(v, t) \equiv p(v, z_i, t | 0, z_j, 0)$  from reset  $V(0) = 0$  in the noise state  $z_j$  to  $V(t) = v$  with  $Z(t) = z_i$  at time  $t > 0$  can be found as solutions of Eq. (19) with the following initial conditions for  $P_{ij}(v, t)$  at  $t = 0$ :

$$P_{ij}(v, 0) = \delta_{ij} \delta(v), \quad (22)$$

where  $\delta_{ij}$  is the Kronecker symbol and  $\delta(v)$  is the Dirac delta function. The probability densities  $P_i(v, t)$  can now be expressed as

$$P_i(v, t) = \sum_{j=1}^3 P_j^{(s)} P_{ij}(v, t). \quad (23)$$

The stationary probabilities  $P_j^{(s)}$  to find the trichotomous noise at reset  $V(0) = 0$  in the state  $z_j$  should be self-consistent, i.e., the initial distribution of noise values at reset has to be equal to the distribution of noise upon firing. From the latter condition and Eq. (19) it follows that

$$P_j^{(s)} = \frac{\mu + z_j}{\mu} p_j. \quad (24)$$

Here the stationary probability  $p_j$  to find noise  $Z(t)$  in the state  $z_j$  is determined by Eq. (2). Equations (19)–(24) can be

reduced to a third-order equation for the probability current (see also Appendix C)

$$\left\{ \left[ \mu \frac{\partial}{\partial v} + \frac{\partial}{\partial t} + v \right] \left[ (\mu^2 - a^2) \frac{\partial^2}{\partial v^2} + \mu \left( 2 \frac{\partial}{\partial t} + v \right) \frac{\partial}{\partial v} + \frac{\partial}{\partial t} \left( \frac{\partial}{\partial t} + v \right) \right] + v a^2 (1 - 2q) \frac{\partial^2}{\partial v^2} \right\} J(v, t) = 0 \quad (25)$$

with the initial conditions

$$\begin{aligned} J(v, 0) &= \mu \left( 1 + \frac{2qa^2}{\mu^2} \right) \delta(v), \\ \frac{\partial}{\partial t} J(v, t)|_{t=0} &= \frac{-2vqa^2}{\mu} \delta(v) - (\mu^2 + 6a^2q) \delta'(v), \\ \frac{\partial^2}{\partial t^2} J(v, t)|_{t=0} &= \frac{2qv^2a^2}{\mu} \delta(v) + 8qva^2 \delta'(v) \\ &\quad + \frac{1}{\mu} [\mu^4 + 2qa^2(6\mu^2 + a^2)] \delta''(v), \end{aligned} \quad (26)$$

and with the boundary conditions

$$J(v < 0, t) = J'(v < 0, t) = J''(v < 0, t) = 0, \quad (27)$$

where the prime denotes the derivative with respect to  $v$ .

The probability current  $J(v, t)$  with conditions (26) and (27) can be obtained by means of the Laplace transformation technique. For the Laplace transform of  $J(v, t)$ , i.e.,

$$\hat{J}(v, s) = \int_0^\infty e^{-st} J(v, t) dt, \quad (28)$$

we obtain from Eqs. (25) and (26) the following ordinary differential equation of third order (see also Appendix C):

$$\begin{aligned} \mu(\mu^2 - a^2) \hat{J}'''(v, s) + [s(3\mu^2 - a^2) + 2v(\mu^2 - qa^2)] \hat{J}''(v, s) \\ + \mu[s(3s + 4v) + v^2] \hat{J}'(v, s) \\ + s(s + v)^2 \hat{J}(v, s) = \hat{f}(v, s) \end{aligned} \quad (29)$$

with

$$\begin{aligned} \hat{f}(v, s) &= \mu(\mu^2 - a^2) \delta''(v) + 2\delta'(v) [\mu^2(s + v) - va^2q] \\ &\quad + (s + v) \left[ \mu(s + v) + \frac{2qa^2s}{\mu} \right] \delta(v). \end{aligned} \quad (30)$$

The solution of Eq. (29) with boundary conditions (27) reads as

$$\hat{J}(v, s) = \left( \sum_{i=1}^3 C_i e^{v\lambda_i} \right) \Theta(v), \quad (31)$$

where the quantities  $\lambda_i$ ,  $i = 1, 2, 3$ , are the roots of the algebraic equation

$$\begin{aligned} \mu(\mu^2 - a^2) \lambda^3 + [s(3\mu^2 - a^2) + 2v(\mu^2 - qa^2)] \lambda^2 \\ + \mu[s(3s + 4v) + v^2] \lambda + s(s + v)^2 = 0, \end{aligned} \quad (32)$$

where the constants  $C_i$  are determined by

$$\begin{aligned} C_i &= s \left[ \lambda_i^2 (\mu^2 - a^2) + 2\mu(s + v) \left( 1 - \frac{qa^2}{\mu^2} \right) \lambda_i + (s + v)^2 \right] \\ &\quad \times \left\{ \lambda_i^2 [2\mu^2(s + v) + s(\mu^2 - a^2) - 2vqa^2] \right. \\ &\quad \left. + 2\lambda_i \mu(s + v)(3s + v) + 3s(s + v)^2 \right\}^{-1}, \end{aligned} \quad (33)$$

and  $\Theta(v)$  is the Heaviside step function. Thus, the Laplace transform  $\hat{w}(s)$  of the ISI density  $w(t)$  is given by

$$\hat{w}(s) = \sum_{i=1}^3 C_i e^{v\lambda_i}. \quad (34)$$

Since the dynamics of voltage evolution, Eq. (1), does not explicitly depend on  $v$ ,  $n$  subsequent passages from  $V = 0$  to  $v_c$ , corresponding to the  $n$ th-order interval  $T_n$  [see Eq. (18)], are by condition (6) equivalent to one passage from  $V = 0$  to  $nv_c$  without reset (see also [18,31]). This property allows us to compute the  $n$ th-order interval distribution by solving the first-passage-time problem with the threshold  $V = nv_c$ , i.e., the Laplace transform  $\hat{w}_n(s)$  of the  $n$ th-order interval density  $w_n(t)$  is determined by

$$\hat{w}_n(s) = \sum_{i=1}^3 C_i e^{nv_c \lambda_i}. \quad (35)$$

We now turn to the description of the  $n$ th-order ISI density  $\tilde{w}_n(t)$  for the subordinated model, Eqs. (11)–(15). The  $n$ th-order interval  $\tilde{T}_n$  at which the membrane potential  $\tilde{V}(t)$  reaches the threshold value  $nv_c$ , starting from the reset state  $\tilde{V}(0) = 0$ , is a random variable which can be defined as

$$\tilde{T}_n = \inf\{t \geq 0 : \tilde{V}(t) > nv_c | \tilde{V}(0) = 0\}. \quad (36)$$

Since  $\tilde{V}(t) = V(S(t))$ , where  $S(t)$  is the inverse of the subordinator  $T(\tau)$ , the following relation holds [48]:

$$\tilde{T}_n \stackrel{d}{=} T(T_n), \quad (37)$$

where  $T_n$  is the first passage time ( $n$ th-order interval) for the parent process  $V(\tau)$ . Here  $\stackrel{d}{=}$  stands for ‘‘equal in distribution.’’ Using Eqs. (37), (9), and the total probability formula [the processes  $V(\tau)$  and  $T(\tau)$  are independent]

$$\tilde{w}_n(t) = \int_0^\infty p(t, \tau) w_n(\tau) d\tau, \quad (38)$$

where  $p(t, \tau)$  is the PDF of  $T(\tau)$ , we can express the Laplace transform of  $\tilde{w}_n(t)$  in the form

$$\hat{\tilde{w}}_n(s) = \hat{w}_n(\phi(s)). \quad (39)$$

This formula is fundamental for the analysis of the behavior of the ISI statistics of the subordinated PIF model (11)–(15).

#### IV. ISI STATISTICS

Neural dynamics can be characterized by several quantities [14,15,26] and here we compute some that are widely used in neuroscientific applications. For model (1) the  $k$ th moment of the  $n$ th-order ISIs  $\langle T_n^k \rangle$ ,  $k = 1, 2, \dots$ , can be expressed via the relation

$$\langle T_n^k \rangle = (-1)^k \frac{d^k}{ds^k} \hat{w}_n(s) |_{s=0}. \quad (40)$$

From this relation and Eqs. (32), (33), and (35) we can derive explicit expressions for the mean  $\langle T_n \rangle$  and central moments  $\langle \Delta T_n^k \rangle = \langle (T_n - \langle T_n \rangle)^k \rangle$ ,  $k = 2, 3$ :

$$\langle T_n \rangle = \frac{nv_c}{\mu}, \quad (41)$$

$$\langle \Delta T_n^2 \rangle = \frac{4qa^2nv_c}{v\mu^3} - \frac{4qa^2}{v^2\mu^4} \left\{ (\mu^2 - 2qa^2) \times [1 - e^{-n\sigma_1} \cosh(n\sigma_2)] - e^{-n\sigma_1} \frac{a[(1-3q)\mu^2 + 2q^2a^2]}{\sqrt{(1-2q)\mu^2 + q^2a^2}} \sinh(n\sigma_2) \right\}, \quad (42)$$

where

$$\sigma_1 = \frac{vv_c(\mu^2 - qa^2)}{\mu(\mu^2 - a^2)}, \quad \sigma_2 = \frac{vv_c a}{\mu(\mu^2 - a^2)} \sqrt{(1-2q)\mu^2 + q^2a^2}, \quad (43)$$

and the third order central moment  $\langle \Delta T_n^3 \rangle$  is presented in Appendix B with Eq. (B1). From these expressions, other statistical measures of the model can be derived, such as the stationary firing rate

$$r = \frac{1}{\langle T_1 \rangle} = \frac{\mu}{v_c}, \quad (44)$$

the coefficient of variation

$$C_v^2 = \frac{\langle \Delta T_1^2 \rangle}{\langle T_1 \rangle^2}, \quad (45)$$

and the skewness

$$\gamma_s = \frac{\langle \Delta T_1^3 \rangle}{(\langle \Delta T_1^2 \rangle)^{3/2}}. \quad (46)$$

Also the serial correlation coefficient (SCC)

$$\rho_n = \frac{\langle I_{n+1}I_1 \rangle - \langle I_{n+1} \rangle \langle I_1 \rangle}{\langle I_1^2 \rangle - \langle I_1 \rangle^2}, \quad (47)$$

which measures the correlation between two intervals with lag  $n$ , is an important statistical characteristic in neuroscientific applications. For stationary spike trains, the variance  $\langle \Delta T_n^2 \rangle$  of the  $n$ th-order interval and the SCC  $\rho_n$  are related as follows [31]:

$$\rho_n = \frac{\langle \Delta T_{n+1}^2 \rangle + \langle \Delta T_{n-1}^2 \rangle - 2\langle \Delta T_n^2 \rangle}{2\langle \Delta T_1^2 \rangle}. \quad (48)$$

Thus, the formulas (42) and (48) allow us to exactly compute the SCC  $\rho_n$ . Moreover, the SCCs and the coefficient of variation are linked to the Fano factor  $F$  in the limit of large spike count windows via the equation [24]

$$F = C_v^2 \left( 1 + 2 \sum_{n=1}^{\infty} \rho_n \right). \quad (49)$$

Let us note that the Fano factor  $F$  is defined as the ratio of variance to the mean of the spike count in the time window  $(0, \infty)$ , and as such it determines the variability of the spike train. Using the variance (42), Eqs. (48) and (49) yield a

simple expression for  $F$ :

$$F = \frac{4a^2q}{v\mu v_c}. \quad (50)$$

This expression has the same form as the  $F$  found for symmetric dichotomous noise in [26]. The only difference is that the factor  $2q$  appears in the numerator. In the case of the subordinated model, Eqs. (11)–(15), the statistical moments of  $n$ th-order ISIs  $\langle \tilde{T}_n^k \rangle$  can be expressed via the relation

$$\langle \tilde{T}_n^k \rangle = (-1)^k \frac{d^{k-1}}{ds^{k-1}} \left[ \left( \frac{d}{ds} \phi(s) \right) \frac{d}{d\phi} \tilde{w}_n(\phi(s)) \right] \Big|_{s=0}, \quad (51)$$

in terms of the moments  $\langle T_n^l \rangle$  for the parent process. Particularly, the output spiking rate  $\tilde{r}$ , the coefficient of variation  $\tilde{C}_v^2$ , and the skewness  $\tilde{\gamma}_s$  are given by

$$\tilde{r} = \frac{\tau}{\langle T(\tau) \rangle} r, \quad \tilde{C}_v^2 = C_v^2 + r\tau C_{T(\tau)}^2, \quad (52)$$

$$\tilde{\gamma}_s = \left( \frac{C_v^2}{\tilde{C}_v^2} \right)^{3/2} \left\{ \gamma_s + \frac{3\tau}{\langle T_1 \rangle} \frac{C_{T(\tau)}^2}{\sqrt{C_v^2}} + \gamma_{T(\tau)} \frac{\tau^2}{\langle T_1 \rangle^2} \left( \frac{C_{T(\tau)}^2}{C_v^2} \right)^{3/2} \right\}, \quad (53)$$

where the mean  $\langle T(\tau) \rangle$ , the coefficient of variation  $C_{T(\tau)}^2$ , and the skewness  $\gamma_{T(\tau)}$  of the subordinator  $T(\tau)$  are determined by Eqs. (16) and (17). For the SCC  $\tilde{\rho}_n$  and the Fano factor  $\tilde{F}$  we obtain

$$\tilde{\rho}_n = \frac{C_v^2}{\tilde{C}_v^2} \rho_n \quad (54)$$

and

$$\tilde{F} = F + r\tau C_{T(\tau)}^2. \quad (55)$$

It should be noted that the formulas for ISI statistics obtained in this section coincide in the particular case of  $q = \frac{1}{2}$  with the results of Refs. [26,41] for a PIF model driven by symmetric dichotomous noise (both with and without subordination).

## V. RESULTS

Before analyzing the behavior of the exact ISI statistics in more detail, it should be noted that all quantities in all figures are dimensionless, with time and voltage scaling determined by  $\tau_0 = 1$  and  $v_c = 1$ .

### A. ISI density

The ISI densities  $w_n(t)$  and  $\tilde{w}_n(t)$  can be found by means of inverse Laplace transforms from Eqs. (35) and (39), respectively. In the case without subordination, it follows from Eqs. (6), (20), and (21) that the support of ISI distribution  $w(t)$  is a finite interval  $[t_1, t_3]$  with

$$t_i = \frac{v_c}{\mu + z_i}, \quad i = 1, 2, 3. \quad (56)$$

The distribution consists of three delta peaks at  $t_i$  and a continuous part between them [cf. also Eq. (B5)]. The delta peaks correspond to realizations of the trichotomous noise in which no switching between noise states occurs while the voltage rises from reset to threshold. The contribution of delta

peaks dominates at small values of the noise switching rate  $\nu < 1/t_3$ , but in the case of high switching rates  $\nu \gg 1/t_1$  only a negligible fraction of the total probability is contained in the delta peaks. The continuous part of  $w(t)$  dominates at small and moderate values of the noise correlation time and results from at least one change in the noise value during the passage of  $V$  from 0 to  $v_c$ . At the long-correlation-time limit  $\nu \rightarrow 0$ , the continuous part is absent and the ISI density

$$w(t) = \sum_{i=1}^3 P_i^{(s)} \delta(t - t_i) \quad (57)$$

is clearly three modal, reflecting that the transitions between states of noise are so rare that the noise values do not change during the passage of  $V$  from 0 to  $v_c$ . In the fast-noise limit  $\nu \rightarrow \infty$ ,  $w(t)$  behaves asymptotically as the ISI density for the PIF model driven by white noise with the intensity  $D = 2qa^2/\nu$ , i.e., as an inverse Gaussian distribution (see also Refs. [13,40]):

$$w(t) \approx \frac{v_c \sqrt{\nu}}{2a\sqrt{\pi} 2qt^3} e^{-\frac{\nu \mu^2 (t-t_2)^2}{8qa^2 t}} \Rightarrow \delta(t - t_2), \quad \nu \rightarrow \infty. \quad (58)$$

In contrast to the parent PIF model considered above the subordinated PIF model predicts an ISI distribution with support on the whole semiaxis  $t \in (0, \infty)$  and the delta peaks are absent. In the case of the small switching rate, where the delta peaks in the ISI density  $w(t)$  are pronounced, the influence of subordination is more expressive for the monofractional Lévy exponent  $\phi(s)$  [see also Eq. (13)]. In this case the PDF of the subordinator  $T(\tau)$  reads as

$$p(t, \tau) = e^{-\delta t} \left( \frac{1 + \delta^\alpha}{\tau} \right)^{\frac{1}{\alpha}} e^{\frac{\tau \delta^\alpha}{1 + \delta^\alpha}} g_\alpha \left[ t \left( \frac{1 + \delta^\alpha}{\tau} \right)^{\frac{1}{\alpha}} \right], \quad (59)$$

where  $\tau_0 = 1$ ,  $0 < \alpha < 1$ , and  $g_\alpha(x)$  is the one-sided  $\alpha$ -stable PDF [54]. A convenient formula for calculating  $g_\alpha(x)$  is represented in Appendix B, Eq. (B10). In the limit where the characteristic exponent  $\alpha$  (sometimes called the memory exponent) tends to 1, the PDF  $p(t, \tau)$  tends to a Dirac delta function, i.e.,

$$p(t, \tau) = \delta \left( t - \frac{\tau}{1 + \delta} \right), \quad \alpha = 1. \quad (60)$$

Thus, at  $\alpha = 1$  the ISI distribution  $\tilde{w}(t)$  behaves like  $w(\tilde{t})$ ,  $\tilde{t} = (1 + \delta)t$ , for the model without subordination. Figures 1(a) and 2(a) show, in the case of the monofractional Lévy exponent, the behavior of  $\tilde{w}(t)$  for different memory exponents  $\alpha$ . By decreasing values of  $\alpha$  the peaks broaden and show an increasing overlap such that the distribution loses its three-modal nature. At moderate and small values of the memory exponent (a strong memory in the corresponding diffusion process) the ISI density is monomodal. For small  $\alpha$ , the maximum of  $\tilde{w}(t)$  corresponds roughly to the maximum of the PDF of the subordinator by  $\tau = t_1$ . Let us note that the position of this maximum shifts in the direction of shorter times as  $\alpha$  decreases. Figures 1(b) and 2(b) display the dependency of  $\tilde{w}(t)$  on the switching rate  $\nu$  for weak memory ( $\alpha = 0.98$ ) and strong memory ( $\alpha = 0.2$ ), respectively.

In the case of weak memory [Fig. 1(b)] the parent process is dominant and at small values of the transition rate  $\nu < 1/t_3$ ,

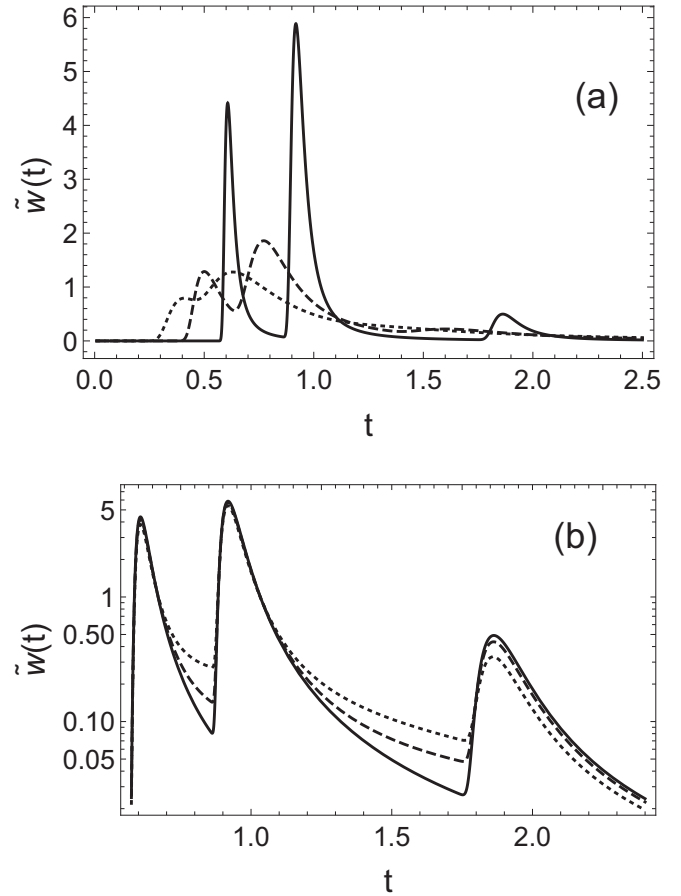


FIG. 1. The ISI density  $\tilde{w}(t)$  for the monofractional Lévy exponent with weak memory, computed from Eqs. (13), (38), (59), (B5), and (B10). The parameter values are  $\mu = v_c = \tau_0 = 1$ ,  $a = 0.5$ ,  $q = 0.2$ ,  $\delta = 0$ . (a) The ISI distribution at different values of the memory exponent  $\alpha$  at a vanishing switching rate  $\nu = 0$ . Solid line:  $\alpha = 0.98$ ; dashed line:  $\alpha = 0.92$ ; dotted line:  $\alpha = 0.85$ . (b) The dependence of  $\tilde{w}(t)$  on small values of the switching rate  $\nu$  at  $\alpha = 0.98$ . Solid line:  $\nu = 0.01$ ; dashed line:  $\nu = 0.1$ ; dotted line:  $\nu = 0.3$ .

$\tilde{w}(t)$  behaves similarly to  $w(t)$ , except that the delta peaks turn into peaks of finite height. Equations (B5) and (B6) show that these peaks are weighted with the exponential factor  $e^{-\nu(1-p_i)t_i}$ , which decreases by increasing  $\nu$ . At strong memory [Fig. 2(b)] the effect of the subordinator is dominant and the ISI distribution  $\tilde{w}(t)$  is monomodal. By increasing  $\nu$ , the position of the maximum of the distribution changes only a little.

The case of bifractional Lévy exponent  $n = 2$  in Eq. (14), with  $\alpha_1 < \alpha_2$ , is considered in Fig. 3. If the values of  $\alpha_1$  and  $\alpha_2$  are sufficiently distinct, then at short times  $t \ll t_1$ , the smaller memory exponent  $\alpha_1$  dominates in the ISI distribution, but in the long-time limit  $t \gg t_3$ , the dynamics of the ISI generation is determined by the greater memory exponent  $\alpha_2$ . Figure 3 demonstrates the emergence of bimodality in the ISI density, induced by the bifractional Lévy exponent. In these parameter regimes the parent process generates monomodal  $w(t)$  with a maximum at  $t \approx v_c/\mu$  [cf. also Eq. (58)]; only a negligible fraction of the total probability is contained in the delta peaks. Hence, the first and second maxima in Fig. 3 are generated

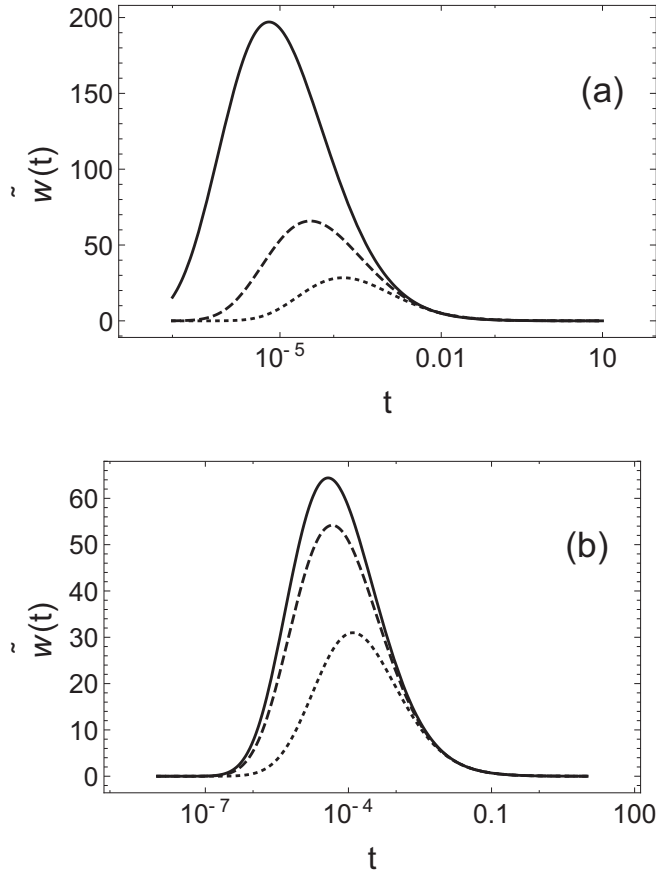


FIG. 2. The case of strong memory. The ISI distribution  $\tilde{w}(t)$  is computed from Eqs. (13), (32)–(34), (39), and (B13). (a) The PDF  $\tilde{w}(t)$  for different values of  $\alpha$  at  $\nu = 0$ . Solid line:  $\alpha = 0.18$ ; dashed line:  $\alpha = 0.2$ ; dotted line:  $\alpha = 0.22$ . (b) The PDF  $\tilde{w}(t)$  for different values of  $\nu$  at  $\alpha = 0.2$ . Solid line:  $\nu = 0.1$ ; dashed line:  $\nu = 1.0$ ; dotted line:  $\nu = 10$ . Other system parameter values are the same as in Fig. 1.

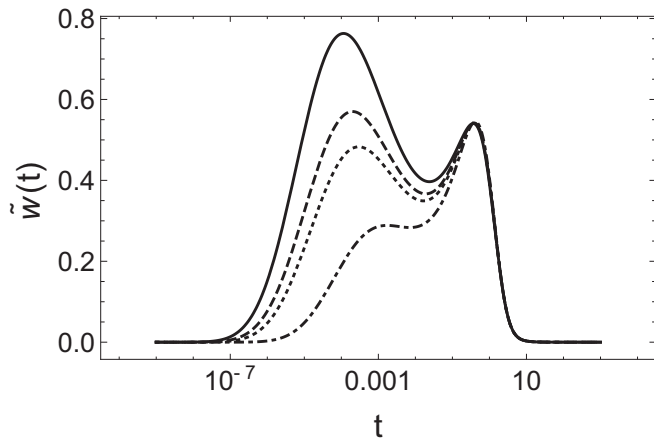


FIG. 3. The behavior of the ISI density  $\tilde{w}(t)$  in the case of the bifractional Lévy exponent, computed from Eqs. (14), (32)–(34), (39), and (B13) at  $n = 2$ . The parameter values are  $\mu = \tau_0 = \nu_c = 1$ ,  $\delta_i = 10^{-10}$ ,  $\alpha_1 = 0.12$ ,  $\alpha_2 = 0.9$ ,  $a = 0.5$ ,  $\eta_1 = 0.25$ , and  $q = 0.4$ . Solid line:  $\nu = 10$ ; dashed line:  $\nu = 15$ ; dotted line:  $\nu = 20$ ; dashed-dotted line:  $\nu = 1000$ .

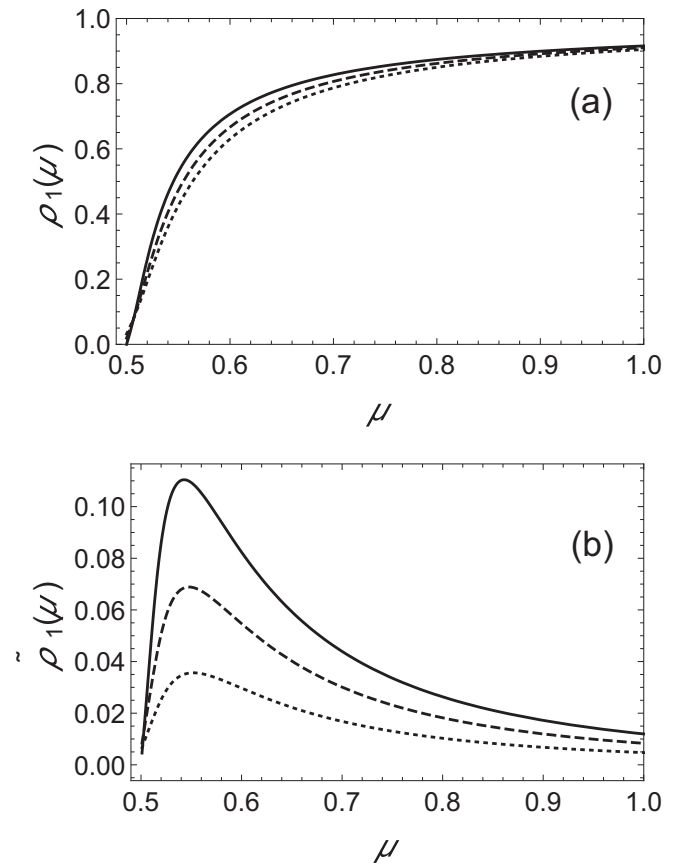


FIG. 4. The serial correlation coefficients  $\rho_1$  and  $\tilde{\rho}_1$  (for lag 1) vs the mean input current  $\mu$  computed at various values of the parameter  $q$ . The curves are computed from Eqs. (54), (52), (48), and (42). The parameter values are  $\tau_0 = \nu_c = 1$ ,  $a = 0.5$ ,  $\delta = 10^{-3}$ ,  $\alpha = 0.12$ , and  $\nu = 0.1$ . (a) The PIF model (1). (b) The subordinated model (12) with a monofractional Lévy exponent, Eq. (13). Solid line:  $q = 0.5$ ; dashed line:  $q = 0.35$ ; dotted line:  $q = 0.2$ . In the limit  $\mu \rightarrow \infty$ , all curves on (a) and (b) tend to 1 and zero, respectively.

by  $\alpha_1$  and  $\alpha_2$ , respectively. Such a subordination-induced bimodality of the ISI density has been previously reported in Ref. [41] for a PIF model driven by dichotomous noise.

### B. ISI variability

In neuroscientific applications the variability of the output spike train is often characterized by the SCC  $\rho_1$ , the Fano factor  $F$ , the skewness  $\gamma_s$ , and the coefficient of variation  $C_v^2$  [see also Eqs. (44)–(49)]. In the following we focus on the dependence of these characteristics on the mean input current  $\mu$ . This is motivated by that  $\mu$  can be easily adjusted in possible experiments. In Figs. 4(a) and 4(b) we depict at several values of the probability  $q$  the typical forms of the graphs  $\rho_1$  and  $\tilde{\rho}_1$  versus  $\mu$ , respectively.

Similarly to the PIF model driven by dichotomous noise ( $q = \frac{1}{2}$ ), considered in [41], in the case of a trichotomous noise the behavior of the SCCs for PIF models with subordination and without subordination is also profoundly different. In the case of subordination the graphs of  $\tilde{\rho}_1$  versus  $\mu$  are clearly monomodal, which indicates that the ISI regularity is maximized at an intermediate value of  $\mu$ . This behavior of  $\tilde{\rho}_1$



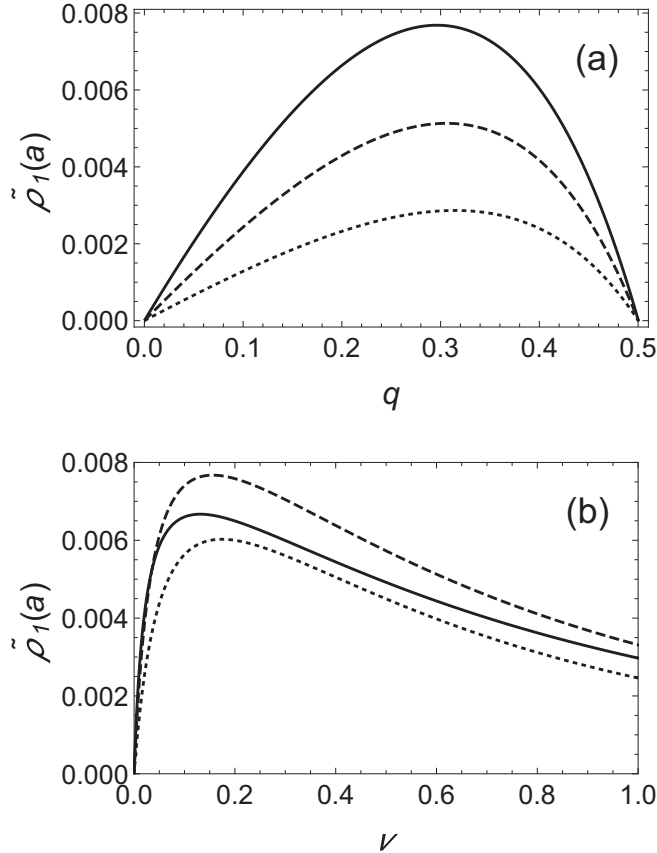


FIG. 5. The dependence of the SCC  $\tilde{\rho}_1(a)$  on the noise parameters  $q$  and  $\nu$  by a monofractional Lévy exponent, computed from Eqs. (13), (42), (52), (54), and (61). Other parameter values are  $\mu = a = 0.5$ ,  $\tau_0 = \nu_c = 1$ , and  $\delta = 10^{-3}$ . (a) The SCC  $\tilde{\rho}_1(a)$  vs  $q$  at various values of the memory exponent  $\alpha$ ,  $\nu = 0.16$ . Solid line:  $\alpha = 0.2$ ; dashed line:  $\alpha = 0.5$ ; dotted line:  $\alpha = 0.8$ . (b) The dependence of  $\tilde{\rho}_1(a)$  on the noise switching rate  $\nu$  at various values of the parameter  $q$ ,  $\alpha = 0.2$ . Solid line:  $q = 0.2$ ; dashed line:  $q = 0.3$ ; dotted line:  $q = 0.4$ . All curves tend to zero as  $\nu \rightarrow \infty$ .

contrasts with that of the model without subordination, where the SCC  $\rho_1$  is always a monotonically increasing function of  $\mu$ . The value of  $\rho_n$  increases from

$$\rho_n(a) \equiv \rho_n|_{\mu=a} = \frac{2a(1-2q)[\sinh(\sigma)]^2}{\{vv_c - (1-2q)a[1 - e^{-2\sigma}]\}} e^{-2\sigma n} \quad (61)$$

with

$$\sigma = \frac{vv_c}{4a(1-q)} \quad (62)$$

to 1 as  $\mu$  increases from  $a$  to  $\infty$ . The main difference between the serial correlation coefficients for models driven by dichotomous and trichotomous noises appears in the limit  $\mu = a$ . In the case of dichotomous noise both  $\rho_n$  and  $\tilde{\rho}_n$  become zero at  $\mu = a$ , reflecting that in this case the threshold is only reached in one of two noise states, i.e., interchange of information between spikes is impossible. But for the PIF model driven by trichotomous noise the SCCs at  $\mu = a$  are different from zero,  $\rho_n(a) \neq 0$  and  $\tilde{\rho}_n(a) \equiv \tilde{\rho}_n(\mu = a) \neq 0$  (except in some limit cases). Since in this case at  $\mu = a$  there are two active states ( $z_1$  and  $z_2$ ), an interchange of information

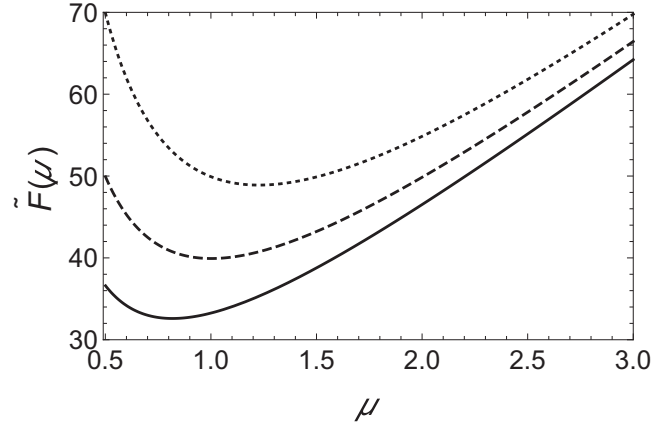


FIG. 6. The Fano factor  $\tilde{F}$  vs the mean input current  $\mu$  at various values of the probability  $q$ , computed from Eqs. (13), (44), (50), and (55). The parameter values are  $\tau_0 = \nu_c = 1$ ,  $a = 0.5$ ,  $\delta = 10^{-3}$ ,  $\alpha = 0.2$ ,  $\nu = 0.015$ . Solid line:  $q = 0.2$ ; dashed line:  $q = 0.3$ ; dotted line:  $q = 0.45$ . In the case of large values of  $\mu$  the Fano factor increases linearly,  $\tilde{F} \sim \mu$ .

between spikes is possible. Figure 5 illustrates how a varying probability  $q$  of the trichotomous noise states changes the value of the quantity  $\tilde{\rho}_1(a)$ .

It is remarkable that the dependencies of  $\tilde{\rho}_1(a)$  on the probability  $q$  and on the noise switching rate  $\nu$  are of a bell-shaped form. The SCC  $\tilde{\rho}_1(a)$  is zero for both extreme values of  $q$ , i.e., at  $q = 0$  and  $\frac{1}{2}$ . Moreover,  $\tilde{\rho}_1(a)$  vanishes also in the fast-noise limit  $\nu \rightarrow \infty$ , and in the long-correlation-time limit  $\nu \rightarrow 0$ , indicating that in these limits the noise cannot carry memory of one ISI to the next. Remarkably, the maximum of  $\tilde{\rho}_1(a)$  increases by decreasing the memory exponent  $\alpha$  [see also Fig. 5(a)]. The behavior of the Fano factor  $\tilde{F}$  at sufficiently small switching rates confirms the statement that the regularity of the spike train is maximized at an intermediate value of  $\mu$  (see also Fig. 6). From Eqs. (44), (50), and (55) one can infer that if

$$\nu < \frac{4q}{\tau C_T^2(\tau)}, \quad (63)$$

the function  $\tilde{F}(\mu)$  demonstrates a minimum at

$$\mu_{ex} = 2a \sqrt{\frac{q}{\nu \tau C_T^2(\tau)}}. \quad (64)$$

Hence, at  $\mu = \mu_{ex}$  the variability of spike counts measured in very large observation time windows is smaller, i.e., long spike trains are more regular than for regimes  $\mu \rightarrow a$  and  $\mu \rightarrow \infty$ .

The minimum gets more pronounced as  $q$  increases. It should be noted that without subordination the Fano factor is a monotonically decreasing function on  $\mu$  [see also Eq. (50)].

Finally, we consider in brief the behavior of the skewness and the coefficient of variation of the ISI distribution. Similarly to the SCC and the Fano factor, these quantities also behave different for models with and without subordination. The main difference appears in the dependencies of  $C_v^2(\mu)$  [or  $\gamma_s(\mu)$ ] and  $\tilde{C}_v^2(\mu)$  [or  $\tilde{\gamma}_s(\mu)$ ] as functions on  $\mu$ . For sufficiently large values of  $\mu$ , both  $\tilde{C}_v^2(\mu)$  and  $\tilde{\gamma}_s(\mu)$  are monotonically

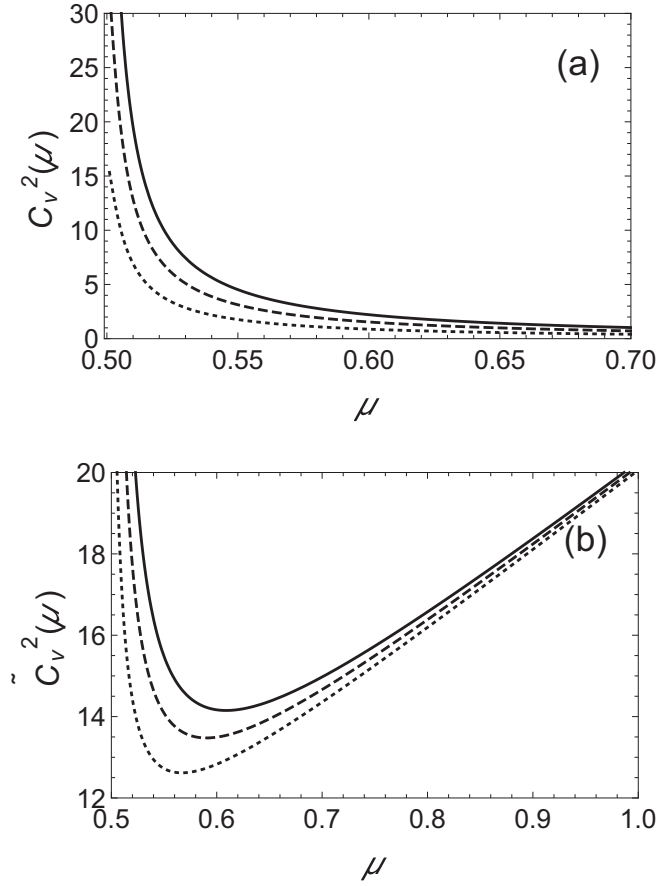


FIG. 7. The coefficients of variation  $C_v^2$  and  $\tilde{C}_v^2$  vs the mean input current  $\mu$  at various values of the trichotomous noise parameter  $q$  [see Eqs. (44), (45), and (52)]. The parameter values are  $\tau_0 = v_c = 1$ ,  $a = 0.5$ ,  $\delta = 10^{-3}$ ,  $\alpha = 0.2$ , and  $\nu = 0.015$ . (a) The PIF model without subordination. (b) The subordinated PIF model with a monofractional Lévy exponent, Eq. (13). Solid line:  $q = 0.5$ ; dashed line:  $q = 0.35$ ; dotted line:  $q = 0.2$ . At  $\mu = a$  all curves tend to a finite value determined by Eqs. (B18) and (52). In the limit  $\mu \rightarrow \infty$  the curves for  $\tilde{C}_v^2$  increase unrestrictedly, but for  $C_v^2$  they tend to zero.

increasing functions  $\tilde{C}_v^2(\mu) \sim \mu$  and  $\tilde{\gamma}_s(\mu) \sim \sqrt{\mu}$ . This contrasts with the case of the PIF model without subordination, where  $C_v^2(\mu)$  and  $\gamma_s(\mu)$  are monotonically decreasing functions on  $\mu$  [see also Eqs. (B21) and (B22)]. In some parameter regimes these statistical measures for the subordinated model show a nonmonotonic dependence on  $\mu$  with a minimum at moderate values of  $\mu$  [see also Figs. 7(b) and 8(b)]. This effect is more pronounced for small transition rates  $\nu$  as well as for large values of the parameter  $q$ . Figures 7 and 8 illustrate how a varying mean input current  $\mu$  changes the coefficient of variation and the skewness of the ISI distribution, respectively.

From Fig. 7 it is seen that the general picture of the behavior of  $C_v^2$  (or  $\tilde{C}_v^2$ ) in the case of dichotomous noise ( $q = \frac{1}{2}$ ) is qualitatively similar to that generated by trichotomous noise ( $q < \frac{1}{2}$ ). In the plot a monotonic increase in the coefficient of variation with an increasing  $q$  can be seen. Hence, compared to models driven by trichotomous noise, the models driven by dichotomous noise generate, by the same values of other system parameters, more variable ISIs. The behavior of  $\tilde{C}_v^2$  for

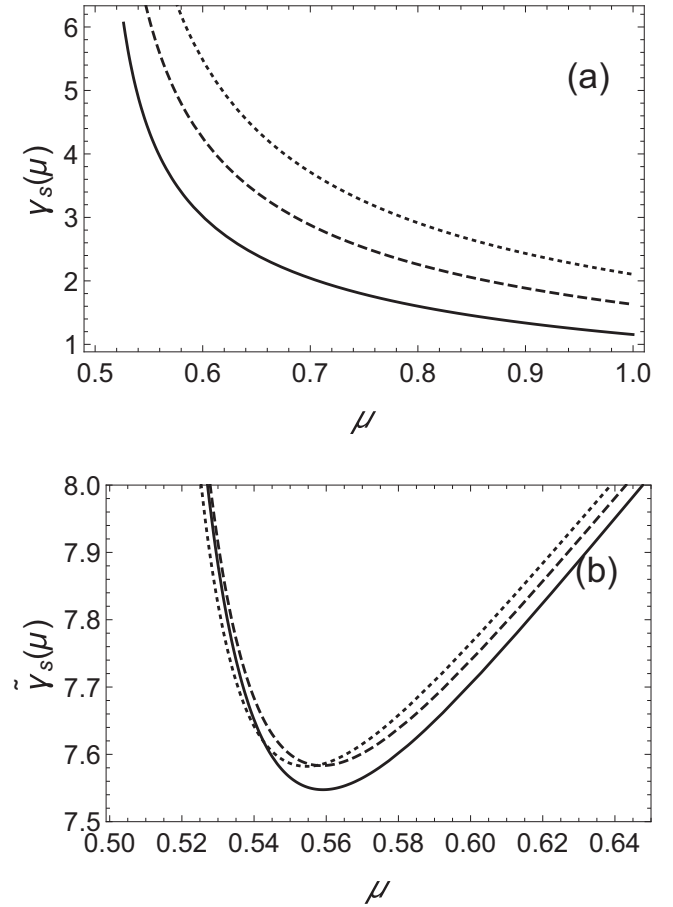


FIG. 8. The skewnesses  $\gamma_s$  and  $\tilde{\gamma}_s$  as functions of the mean input current  $\mu$  at various values of the noise parameter  $q$ . The curves are computed from Eqs. (13), (16), (17), (44)–(46), (52), (53), and (B1). (a) The PIF model without subordination. (b) The PIF model with subordination. All model parameters and the notations for lines are the same as for Fig. 7. The finite values of  $\gamma_s$  and  $\tilde{\gamma}_s$  at  $\mu = a$  are determined by Eqs. (B19) and (53). In the limit  $\mu \rightarrow \infty$  all curves  $\tilde{\gamma}_s(\mu)$  increase in proportion to  $\sqrt{\mu}$ , but the curves  $\gamma_s(\mu)$  tend to zero.

a PIF model driven by dichotomous noise has been previously considered in more detail in Ref. [41].

For reference, let us mention that the class of renewal point processes [55] has gained popularity in theoretical neuroscience. In a renewal model the intervals between successive spikes are independent and identically distributed. For renewal models the spike count variability depends solely on the dispersion of ISIs and it holds that  $F = C_v^2$  [55,56]. Particularly, for a Poisson process  $F = C_v^2 = 1$ . Processes with  $F < 1$  are thus considered less variable than Poisson processes, whereas those with  $F > 1$  are more variable. In the particular case of a periodic spike train both characteristics  $F$  and  $C_v^2$  vanish, i.e.,  $F = C_v^2 = 0$ . Since in both our models the interspike intervals are no longer independent, but exhibit serial dependencies, the relation  $F = C_v^2$  will change:  $F$  is not in general equal to  $C_v^2$  [see also Eqs. (49) and (54)]. Thus, in the parameter regimes exposed in Figs. 6 and 7 the subordinated model predicts much more variable spike trains than for a Poisson process. Moreover, it is seen that  $\tilde{C}_v^2$  and  $\tilde{F}$  as functions of  $\mu$  increase linearly by sufficiently large

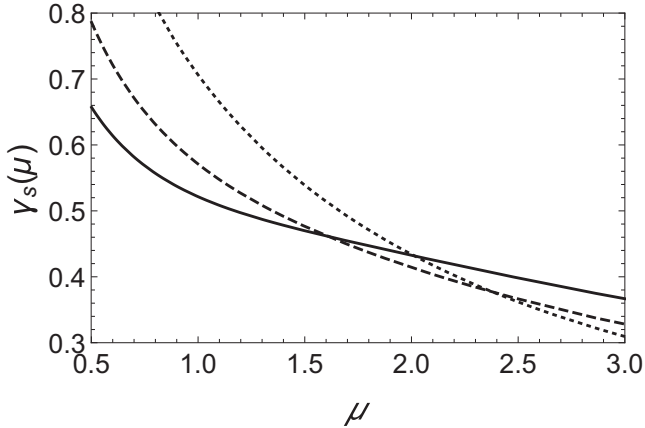


FIG. 9. The dependence of the skewness  $\gamma_s$  on the mean input current  $\mu$  computed from Eqs. (42), (46), and (B1) at various values of the noise parameter  $q$ . The model parameters are  $a = 0.5$ ,  $v_c = 1$ , and  $v = 8$ . Solid line:  $q = 0.15$ ; dashed line:  $q = 0.25$ ; dotted line:  $q = 0.5$ .

values of  $\mu$ ,  $\mu \gg a$  [see also Eqs. (50), (55), and (B21)]. This finding may be important in view of possible experiments. As pointed out in Ref. [41], such a linear dependence on  $\mu$  can indicate a subordination in the spike generation process of a neuron. It should be noted that in the regime  $\mu \gg a$  the spike generation process possesses a renewal character with the ISI PDF  $\tilde{w}(t) \approx p(t, v_c/\mu)$  [see Eqs. (9) and (38)]; in this regime the parent process generates an approximately periodic spike train with  $w(\tau) \approx \delta(\tau - v_c/\mu)$ . Notably, in the particular case when the memory exponent  $\alpha = \frac{1}{2}$ , the ISI PDF tends at  $\mu \gg a$  to an inverse Gaussian distribution

$$\tilde{w}(t) \approx \frac{1}{2\sqrt{\pi}t^{3/2}} \left( \frac{v_c}{\mu\sqrt{\tau_0}[1 + \sqrt{\tau_0\delta}]} \right) \times \exp \left\{ -\frac{\delta}{t} \left( t - \frac{v_c}{2\mu\sqrt{\delta\tau_0}[1 + \sqrt{\delta\tau_0}]} \right)^2 \right\}, \quad (65)$$

which is one of the most widely used distributions for modeling ISI lengths [57].

In the parameter regimes given in Fig. 8, i.e., when the noise switching rate is small,  $v \ll (\mu - a)/v_c$ , the skewness  $\gamma_s(\mu)$  behaves as

$$\gamma_s(\mu) = \frac{\sqrt{2}a}{\sqrt{q(\mu^2 - a^2)}} + O\left(\frac{vv_c}{\mu - a}\right), \quad \mu > a + vv_c \quad (66)$$

with

$$\gamma_s(a) \approx 3\sqrt{\frac{a}{2qvv_c(1 - q)}}, \quad \mu = a. \quad (67)$$

Equation (66) implies that the ISI distribution generated by trichotomous noise is (for sufficiently small switching rates) more asymmetric than the one driven by dichotomous noise. In Fig. 9 the case of a relatively high switching rate ( $v \gg a/2qv_c$ ) is considered. It is remarkable that relying on Eqs. (B15) and (B22) one can discern two regimes  $\mu < 2qv_c v$  and  $\mu > 2qv_c v$  for the behavior of the skewness  $\gamma_s(\mu)$ . In the

case of  $\mu < 2qv_c v$ ,  $\gamma_s(\mu)$  behaves by increasing  $q$  as

$$\gamma_s(\mu) \approx \frac{6\sqrt{q}a}{\sqrt{v\mu v_c}}, \quad \mu \ll 2qv_c v \quad (68)$$

i.e., by increasing the noise parameter  $q$  (other parameters are fixed) the asymmetry of the ISI distribution grows, but in the case of  $\mu > 2qv_c v$  it decreases by increasing  $q$ ,

$$\gamma_s(\mu) \approx \frac{\sqrt{2}a}{\mu\sqrt{q}}, \quad \mu \gg 2qv_c v. \quad (69)$$

Thus, for sufficiently small values of  $\mu$  the ISI distribution for the model driven by trichotomous noise is more symmetric than for the model driven by dichotomous noise, but in the case of  $\mu > 2qv_c v$  the situation is opposite.

Some further insight about the asymptotic behavior of parameters  $\tilde{C}_v^2$  and  $\tilde{\gamma}_s$  at various limits can be obtained from Appendix B. The formulas presented in this Appendix may be also useful for analysis of experimental data. For example, the asymptotic formulas (B21) and (B22) give, under the assumption that the presented subordinated model with the Lévy exponent given by Eq. (13) is relevant, simple expressions for estimation of the input parameters  $\alpha$  and  $\delta$  from the output data. Namely, if  $\mu \gg a$ , it follows that

$$\alpha \approx \frac{\tilde{\gamma}_s - 2\tilde{C}_v}{\tilde{\gamma}_s - \tilde{C}_v}, \quad \delta \approx \frac{\tilde{r}}{\tilde{C}_v(\tilde{\gamma}_s - \tilde{C}_v)}, \quad (70)$$

where the output spiking rate  $\tilde{r}$ , the coefficient of variation  $\tilde{C}_v$ , and the skewness  $\tilde{\gamma}_s$  can be obtained from experimental data. Finally, we note that time  $t$  and voltage  $v$  in all figures are measured in units of the membrane time constant  $\tau_0$  and of the threshold potential  $v_c$ , respectively. Thus, for the typical value of  $\tau_0 = 10$  ms the switching rate  $v = 0.015$  (see Figs. 6–8) corresponds to 1.5 Hz, which is close to the range of the values (2–3) Hz estimated for the transition rates from up to down states for neurons in the striatum of rats [25,58]. In Ref. [58] it is also found that for corticostriatal and striatal neurons, the coefficients of variation of ISIs range from 1.0 to 1.9. For reference, in our model the value  $C_v \approx 1.8$  can be achieved, e.g., in the parameter regime:  $v = 0.015$ ,  $v_c = \tau_0 = 1$ ,  $q = 0.5$ ,  $\alpha = 0.2$ ,  $\delta = 10^{-2}$ ,  $a = 0.1$ , and  $\mu = 0.2$ . Of course, detailed experimental investigations are required for any conclusion on the relevance of the model, which at this moment remains as a speculation only.

## VI. CONCLUSIONS

We have studied, in a tonically firing regime, the effect of input trichotomous noise on the firing statistics of a PIF neuron model. Using the Laplace transform of the output ISI distribution, we have derived exact analytical expressions of statistical measures for the output spike train, such as the serial correlation coefficient, the Fano factor for large observation time windows, the coefficient of variation, and the skewness. Motivated by studies of the dynamics of a subordinated model of dichotomous noise driven neurons [41], we have also considered a trichotomous noise driven PIF model inserting a random operational time in the form of an inverse strictly increasing Lévy-type subordinator. Exact formulas for spike train statistics are obtained also in this case.

As our main result, we have established that the input trichotomous noise is, aside from the dichotomous noise, another example of a driving non-Gaussian colored noise that leads to exact results for the statistical measures of a PIF model. Moreover, the dynamics of the generalized model with subordination considered in this paper (see also Refs. [40,41]) is a highly non-Markovian process, which makes the model promising, since in general the determination of ISI statistics for a non-Markovian process is very difficult and so far various approximations or extensive computer simulations have been used [21,23].

Particularly, we have shown that in some parameter regimes both models predict a three-modal structure of the ISI density for small switching rates  $\nu$  of the input noise. For the model without subordination, in the limit of high switching rate the distribution approaches an inverse Gaussian, i.e., the system behaves similarly to the PIF model driven by white noise. In the particular case of the monofractional Lévy exponent (13), which in the subordinated PIF model describes a subdiffusive evolution of the subthreshold membrane potential, the three-modal structure of ISI density is more pronounced as the memory exponent  $\alpha$  tends to 1 (i.e., in the case of a low memory). By decreasing values of  $\alpha$  the peaks broaden and show an increasing overlap such that the distribution loses its three-modal structure and becomes monomodal.

Considering other statistical measures of the output spike train we focused on their dependence on the mean input current  $\mu$ . This is motivated by that  $\mu$  can easily be adjusted in possible experiments. As a rule, these statistical measures behave qualitatively similarly to the corresponding characteristics of PIF models driven by dichotomous noise. In comparison to the PIF model driven by dichotomous noise considered in Refs. [26,41], the most important findings are the decreased variability of the output spike train as well as the increased skewness of the ISI distribution at the same values of system parameters. Exceptions are the behaviors of the serial correlation coefficient and the skewness in the neighborhood of  $\mu = a$ , where  $a$  is the noise amplitude. In the case of input dichotomous noise the output SCC ( $\rho_1$ ) always becomes zero at  $\mu = a$ , reflecting that in this case the firing threshold is only reached in one of the two noise states, i.e., interchange of information between spikes is impossible. But for models driven by trichotomous noise the SCC at  $\mu = a$  is finite [ $\rho_1(a) \neq 0$ ] since in this case there are two active noise states at  $\mu = a$  and interchange of information between spikes is possible. It is important to note that in the case of the subordinated model the dependence of the SCC  $\rho_n(a)$  on the noise parameter  $q \in (0, \frac{1}{2})$  (for dichotomous noise  $q = \frac{1}{2}$ ) exhibits a bell-shaped form:  $\rho_n(a) = 0$  at  $q = 0$  and at  $q = \frac{1}{2}$ .

The next interesting result is that for sufficiently high values of the noise switching rate  $\nu$ , one can discern two regimes for the behavior of the ISI skewness  $\gamma_s(\mu)$ :  $\mu < \mu_c$  and  $\mu > \mu_c$  with a critical value  $\mu_c$ , which can be roughly estimated as  $\mu_c \approx 2q\nu v$ , where  $v_c$  is the threshold potential of the neuron membrane. In the case of  $\mu < \mu_c$ , by increasing the noise parameter  $q$  (the other parameters are fixed) the asymmetry of the ISI distribution grows, but for  $\mu > \mu_c$  it decreases by increasing  $q$ . Finally, we note that the subordinated model predicts in the large  $\mu$  limit a specific behavior of the

skewness: by increasing  $\mu$  the skewness increases unlimited in proportion to  $\sqrt{\mu}$  [see also Eq. (B22)]. Contrary to that, the ISI skewness for the model without subordination always tends to zero if  $\mu \rightarrow \infty$ . Here we emphasize that the behavior of the skewness for a subordinated neuronal model has not been considered previously.

We remark that in any realistic neural model, attaining the ISI PDF should not be considered as the final achievement, but rather as a starting point toward the description of a neuron's output. Since the trichotomous noise is more flexible than the dichotomous noise and the model is robust enough to modify the Lévy exponent, we hope that the models considered here may be useful to shed some new light on the modeling of dynamical aspects of real neurons. However, future investigations are needed to clarify the biophysical background of the models suggested in this paper.

Finally, we believe that the results discussed in this paper can be a good starting point for investigations by numerical simulations of more elaborated model systems for neuronal dynamics in networks, and can also be of interest in other fields where trichotomous noise is relevant for modeling a system.

## ACKNOWLEDGMENTS

This paper was supported by the Center of Excellence in Behavioral and Natural Sciences, Tallinn University, Estonia, under the project TU TEE. The project is supported by the European Union through the European Regional Development Fund. The authors would like to thank the anonymous reviewers for their valuable comments.

## APPENDIX A: TRICHOTOMOUS NOISE

In this Appendix we summarize in brief the main properties of the trichotomous noise. All these properties are taken from Ref. [3].

The trichotomous process  $Z(t)$  is a stationary Markovian process that consists of jumps between three values  $a$ ,  $0$ , and  $-a$ . The jumps follow in time according to a Poisson process, while the values occur with the stationary probabilities presented in Eq. (2). The mean value of  $Z(t)$  and the correlation function are given by Eq. (3). The kurtosis  $\kappa$  of the noise  $Z(t)$  proves to be a simple expression of the probability  $q$  [see Eq. (2)]:

$$\kappa := \frac{\langle Z^4(t) \rangle}{\langle Z^2(t) \rangle^2} - 3 = \frac{1}{2q} - 3. \quad (\text{A1})$$

The probabilities  $W_n(t)$  that  $Z(t)$  is in the state  $n \in \{1, 2, 3\}$ ,  $z_1 = a$ ,  $z_2 = 0$ , and  $z_3 = -a$ , at time  $t$  evolve according to the master equation

$$\frac{d}{dt} W_n(t) = \nu \sum_{m=1}^3 S_{nm} W_m(t), \quad (\text{A2})$$

where

$$S_{nm} = \begin{bmatrix} q-1 & q & q \\ 1-2q & -2q & 1-2q \\ q & q & q-1 \end{bmatrix}. \quad (\text{A3})$$

The transition probabilities  $T_{ij} = p(z_i, t + \tau | z_j, t)$  between the states  $z_n, n = 1, 2, 3$ , can be represented by means of a transition matrix  $T_{ij}$  of the trichotomous process as follows:

$$T_{ij} = \delta_{ij} + (1 - e^{-\nu\tau})S_{ij}, \tag{A4}$$

where  $\delta_{ij}$  is the Kronecker symbol.

Taking the limit where the noise amplitude  $a \rightarrow \infty$  and the switching rate  $\nu \rightarrow \infty$  such that  $D = 4qa^2/\nu$  is finite, we can have a delta-correlated noise, which has the properties of white Gaussian noise with zero mean and a completely flat spectrum.

**APPENDIX B: FORMULAS FOR THE PIF MODEL DRIVEN BY TRICHOTOMOUS NOISE**

In this Appendix, we describe some formulas which are absent from the main text, but are referred to in Sec. V.

**1. Third order central moment**

From Eqs. (32)–(35), and (40) it follows that

$$\begin{aligned} \langle \Delta T_n^3 \rangle &= \frac{12v_c n q a^4}{v^2 \mu^5} \{4q + e^{-\sigma_1 n} [A_1 \cosh(n\sigma_2) \\ &- A_2 \sinh(n\sigma_2)]\} + \frac{12a^4 q}{v^3 \mu^4} \{2B_1 [1 \\ &- e^{-n\sigma_1} \cosh(n\sigma_2)] - B_2 e^{-n\sigma_1} \sinh(n\sigma_2)\}, \end{aligned} \tag{B1}$$

where

$$A_1 = \frac{q[3(1 - 2q)\mu^2 + 4q^2 a^2]}{[(1 - 2q)\mu^2 + q^2 a^2]}, \tag{B2}$$

$$A_2 = \frac{[\mu^2(1 - 2q) + 4q^2 a^2]}{a\sqrt{(1 - 2q)\mu^2 + q^2 a^2}}, \tag{B2}$$

$$B_1 = 1 - 6q + 8\frac{q^2 a^2}{\mu^2}, \tag{B3}$$

$$\begin{aligned} B_2 &= \frac{1}{a\sqrt{(1 - 2q)\mu^2 + q^2 a^2}} \left\{ (\mu^2 - a^2) \left[ 2 - 5q \right. \right. \\ &+ \left. \frac{16a^2 q^3}{\mu^2} + \frac{a^2 q^3}{[(1 - 2q)\mu^2 + q^2 a^2]} \right] \\ &+ \left. 2a^2(1 - q)(1 - 2q)(1 - 4q) \right\}, \end{aligned} \tag{B4}$$

and the quantities  $\sigma_1$  and  $\sigma_2$  are determined by Eqs. (43).

**2. ISI density at the long-correlation time**

In the case of a small switching rate of noise  $Z(t), \nu < 1/t_3$ , the inverse Laplace transform of Eq. (34) gives

$$\begin{aligned} w(t) &= e^{-\nu t} \sum_{i=1}^3 C_i^* \{ \delta(t - t_i) + [g_i(a) \\ &+ (t - t_i)h_i(a)]\Theta(t - t_i) \} + O(\nu^3), \end{aligned} \tag{B5}$$

where

$$t_i := \frac{v_c}{\mu + z_i}, \quad C_i^* = P_i^{(s)} e^{\nu t_i p_i} \tag{B6}$$

[see also Eqs. (2), (24), and (56)],

$$\begin{aligned} g_2(a) &= -4qv, \\ g_1(a) = g_3(-a) &= \frac{\nu}{a} [\mu(2 - 3q) - aq] \\ &+ \frac{\nu^2 q v_c}{2a} (2 - 3q), \end{aligned} \tag{B7}$$

$$h_2(a) = -\frac{2\nu^2 q}{a^2} [3\mu^2(1 - 2q) + 2a^2(1 - 3q)], \tag{B8}$$

and

$$\begin{aligned} h_1(a) = h_3(-a) &= \frac{\nu^2}{a^2} \left\{ (1 - 2q)[3\mu(1 - 2q)(\mu + a) \right. \\ &- a(\mu(1 - q) + aq)] + \left. \frac{aq^2}{2}(\mu - a) \right\}. \end{aligned} \tag{B9}$$

Equation (B5) is valid for  $t_1 \leq t \leq t_3$ . The ISI density  $w(t)$  is zero for both shorter and longer times  $t$ .

**3. Formulas for the calculation of PDFs of subordinators**

As shown by Ref. [54], the one-sided  $\alpha$ -stable PDF  $g_\alpha(x)$  can be transformed into a nonoscillating function integral that is convenient for numerical calculations:

$$\begin{aligned} g_\alpha(x) &= \frac{\alpha}{1 - \alpha} x^{-\frac{1}{1-\alpha}} \\ &\times \int_0^1 d\xi A(\xi; \alpha) \exp[-x^{-\frac{\alpha}{1-\alpha}} A(\xi; \alpha)], \end{aligned} \tag{B10}$$

with

$$A(\xi; \alpha) = \frac{\sin[(1 - \alpha)\pi\xi][\sin(\alpha\pi\xi)]^{\frac{\alpha}{1-\alpha}}}{[\sin(\pi\xi)]^{\frac{1}{1-\alpha}}}, \tag{B11}$$

where  $0 < \alpha < 1$ . Equations (B10), (B11), and (59) enable to calculate the PDF of the monofractional subordinator  $T(\tau)$  determined by Eq. (13).

In the multifractional case of the Lévy exponent (14) a convenient formula for the calculation of  $\tilde{w}(t)$  can be obtained if  $0 < \min\{\alpha_i; i = 1, 2, \dots, n\} < 0.5$ , [41]. In this case the appropriate contour in the complex plane  $\{s\}$  for the evaluation of the inverse Laplace transform of  $e^{-\tau\phi(s)}$  can be transformed to the Hankel contour with a cut along the real negative semi-axis [in the half-plane  $\text{Re}(s) < 0$  the poles are absent]. Thus, the PDF of the subordinator is given by

$$p(t, \tau) = -\frac{1}{\pi} \int_\delta^\infty dr e^{-rt} \text{Im}[e^{-\tau\phi(-r)}], \tag{B12}$$

$0 < \min\{\alpha_i\} < 0.5$ . Now, from Eqs. (B12) and (38) it follows:

$$\tilde{w}(t) = -\frac{1}{\pi} \int_\delta^\infty dr e^{-rt} \text{Im}[\tilde{w}(-r)] \tag{B13}$$

[see also Eqs. (35) and (39)].

**4. Asymptotic behavior of the skewness and the coefficient of variation**

Here we present some formulas for  $C_v^2, \tilde{C}_v^2, \gamma_s$ , and  $\tilde{\gamma}_s$  at the limits of fast noise ( $\nu \rightarrow \infty$ ), long-correlation time of noise

( $\nu \rightarrow 0$ ), large values of mean input current ( $\mu \rightarrow \infty$ ), and at  $\mu \rightarrow a$ , obtained from Eqs. (42), (52), (53), and (B1).

(i) In the fast-noise limit ( $\nu \rightarrow \infty$ ) these statistical characteristics are given by

$$C_v^2 = \frac{4qa^2}{\nu v_c \mu}, \quad \tilde{C}_v^2 = \frac{\mu \tau}{v_c} C_{T(\tau)}^2, \quad (\text{B14})$$

and

$$\gamma_s = 3\sqrt{C_v^2} = \frac{6\sqrt{qa}}{\sqrt{\nu \mu v_c}}, \quad \tilde{\gamma}_s = \sqrt{\frac{\mu \tau}{v_c}} \gamma_{T(\tau)}, \quad (\text{B15})$$

where  $C_{T(\tau)}^2$  and  $\gamma_{T(\tau)}$  are the coefficient of variation and the skewness of the subordinator  $T(\tau)$ , respectively [see also Eqs. (16) and (17)].

(ii) In the limit  $\nu \rightarrow 0$  these quantities read as

$$C_v^2 = \frac{2qa^2}{\mu^2 - a^2}, \quad \tilde{C}_v^2 = \frac{2qa^2}{\mu^2 - a^2} + \frac{\tau}{v_c} C_{T(\tau)}^2 \mu, \quad (\text{B16})$$

and

$$\gamma_s = \frac{\sqrt{2}a}{\sqrt{q(\mu^2 - a^2)}}. \quad (\text{B17})$$

In this limit the skewness  $\tilde{\gamma}_s$  for the subordinated process is now determined by Eq. (53).

(iii) At  $\mu \rightarrow a$  the behaviors of  $C_v^2$  and  $\gamma_s$  are given by

$$C_v^2 = \frac{4qa}{\nu v_c} \left\{ 1 - \frac{(1-2q)a}{\nu v_c} [1 - e^{-2\sigma}] \right\}, \quad (\text{B18})$$

and

$$\gamma_s = \frac{24qa^2}{\nu^2 v_c^2 (C_v^2)^{3/2}} \left\{ 2q - \frac{(1-2q)^3}{4(1-q)^2} e^{-2\sigma} + \frac{a(1-2q)(1-4q)}{\nu v_c} [1 - e^{-2\sigma}] \right\}, \quad (\text{B19})$$

where

$$\sigma = \frac{\nu v_c}{4a(1-q)}. \quad (\text{B20})$$

from which it is easy to find Eq. (25).

## 2. Derivations of Eqs. (29) and (30)

To find Eqs. (29) and (30), we start from Eq. (25). Using for a Laplace transform of the function  $g(t)$  the notation

$$\hat{g}(s) = \hat{L}_s(g(t)) = \int_0^\infty e^{-st} g(t) dt \quad (\text{C8})$$

The quantities  $\tilde{C}_v^2$  and  $\tilde{\gamma}_s$  can now be found from Eqs. (52) and (53), respectively.

(iv) In the case of  $\mu \rightarrow \infty$ , the asymptotic behavior of  $C_v^2$  and  $\gamma_s$  can be described as follows:

$$C_v^2 = \frac{2qa^2}{\mu^2}, \quad \tilde{C}_v^2 = \frac{\tau \mu}{v_c} C_{T(\tau)}^2, \quad (\text{B21})$$

and

$$\gamma_s = \frac{\sqrt{2}a}{\mu \sqrt{q}}, \quad \tilde{\gamma}_s = \gamma_{T(\tau)} \sqrt{\frac{\tau \mu}{v_c}}. \quad (\text{B22})$$

Note that the formulas for  $\tilde{C}_v^2$  and  $\tilde{\gamma}_s$  coincide with the corresponding formulas in the limit  $\nu \rightarrow \infty$ .

## APPENDIX C: DERIVATION OF EQS. (25), (29), AND (30)

### 1. Derivation of Eq. (25)

By the change

$$P = P_1 + P_2 + P_3, \quad P_2 = P_2, \\ J = (\mu + a)P_1 + \mu P_2 + (\mu - a)P_3. \quad (\text{C1})$$

Equation (19) can be transformed into the system of equations

$$\frac{\partial}{\partial t} P = -\frac{\partial}{\partial v} J, \quad (\text{C2})$$

$$\hat{M} P_2 = \nu(1-2q)P, \quad (\text{C3})$$

$$\left[ \hat{M} - a \frac{\partial}{\partial v} \right] J = \left[ (\mu + a) \left( \hat{M} - a \frac{\partial}{\partial v} \right) - \nu a \right] P + a^2 \frac{\partial}{\partial v} P_2, \quad (\text{C4})$$

where the operator  $\hat{M}$  is defined by

$$\hat{M} = \frac{\partial}{\partial t} + \mu \frac{\partial}{\partial v} + \nu. \quad (\text{C5})$$

Using Eqs. (C3) and (C4) we obtain

$$\hat{M} \left[ \hat{M} - a \frac{\partial}{\partial v} \right] J = \hat{M} \left[ (\mu + a) \left( \hat{M} - a \frac{\partial}{\partial v} \right) - \nu a \right] P \\ + \nu(1-2q)a^2 \frac{\partial}{\partial v} P. \quad (\text{C6})$$

Now, this equation and Eq. (C2) give

$$\frac{\partial}{\partial t} \hat{M} \left[ \hat{M} - a \frac{\partial}{\partial v} \right] J = - \left\{ \hat{M} \left[ (\mu + a) \left( \hat{M} - a \frac{\partial}{\partial v} \right) - \nu a \right] + \nu(1-2q)a^2 \frac{\partial}{\partial v} \right\} \frac{\partial}{\partial v} J, \quad (\text{C7})$$

and the classical formula for the Laplace transform of derivatives

$$\hat{L}_s \left( \frac{d^n}{dt^n} g(t) \right) = s^n \hat{g}(s) - \sum_{k=0}^{n-1} s^k \left[ \frac{d^{n-k-1}}{dt^{n-k-1}} g(t) \right]_{t=0}, \quad (\text{C9})$$

the Laplace transform of Eq. (25) gives

$$\mu(\mu^2 - a^2) \hat{J}'''(v, s) + [s(3\mu^2 - a^2) + 2\nu(\mu^2 - qa^2)] \hat{J}''(v, s) \\ + \mu[s(3s + 4\nu) + \nu^2] \hat{J}'(v, s) + s(s + \nu)^2 \hat{J}(v, s) = \hat{f}(v, s), \quad (\text{C10})$$

with

$$\begin{aligned} \hat{f}(v, s) = & s^2 J(v, 0) + s[3\mu J'(v, 0) + \dot{J}(v, 0) + 2\nu J(v, 0)] \\ & + [(3\mu^2 - a^2)J''(v, 0) + 3\mu\dot{J}'(v, 0) \\ & + 4\nu\mu J'(v, 0) + \ddot{J}(v, 0) + 2\nu\dot{J}(v, 0) + \nu^2 J(v, 0)], \end{aligned} \quad (\text{C11})$$

where the prime denotes the derivative with respect to  $v$  and

$$\dot{J}(v, 0) = \left[ \frac{\partial}{\partial t} J(v, t) \right]_{t=0}, \quad \ddot{J}(v, 0) = \left[ \frac{\partial^2}{\partial t^2} J(v, t) \right]_{t=0}. \quad (\text{C12})$$

Thus, taking into account the initial conditions (26) Eq. (C11) reduces to the expression (30).

- 
- [1] R. Benzi, A. Sutera, and A. Vulpiani, The mechanism of stochastic resonance, *J. Phys. A: Math. Gen.* **14**, 453 (1981).
- [2] L. Gammaitoni, P. Hänggi, P. Jung, and F. Marchesoni, Stochastic resonance, *Rev. Mod. Phys.* **70**, 223 (1998).
- [3] E. Soika, R. Mankin, and J. Priimets, Generalized Langevin equation with multiplicative trichotomous noise, *Proc. Estonian Acad. Sci.* **61**, 113 (2012).
- [4] M. O. Magnasco, Forced Thermal Ratchets, *Phys. Rev. Lett.* **71**, 1477 (1993).
- [5] P. Reimann, Brownian motors: Noisy transport far from equilibrium, *Phys. Rep.* **361**, 57 (2002).
- [6] I. Bena, C. Van den Broeck, R. Kawai, and K. Lindenberg, Nonlinear response with dichotomous noise, *Phys. Rev. E* **66**, 045603(R) (2002).
- [7] R. Mankin, A. Haljas, R. Tammelo, and D. Martila, Mechanism of hypersensitive transport in tilted sharp ratchets, *Phys. Rev. E* **68**, 011105 (2003).
- [8] F. Höfling and T. Franosch, Anomalous transport in the crowded world of biological cells, *Rep. Prog. Phys.* **76**, 046602 (2013).
- [9] E. W. Montroll and G. H. Weiss, Random walks on lattices. II, *J. Math. Phys.* **6**, 167 (1965).
- [10] S. C. Kou and X. S. Xie, Generalized Langevin Equation with Fractional Gaussian Noise: Subdiffusion within a Single Protein Molecule, *Phys. Rev. Lett.* **93**, 180603 (2004).
- [11] R. Mankin, K. Laas, N. Lumi, and A. Rekker, Cage effect for the velocity correlation functions of a Brownian particle in viscoelastic shear flows, *Phys. Rev. E* **90**, 042127 (2014).
- [12] R. Mankin, K. Laas, T. Laas, and S. Paekivi, Memory effects for a stochastic fractional oscillator in a magnetic field, *Phys. Rev. E* **97**, 012145 (2018).
- [13] G. L. Gerstein and B. Mandelbrot, Random walk models for the spike activity of a single neuron, *Biophys. J.* **4**, 41 (1964).
- [14] A. N. Burkitt, A review of the integrate-and-fire neuron model: I. Homogeneous synaptic input, *Biol. Cybern.* **95**, 1 (2006).
- [15] A. N. Burkitt, A review of the integrate-and-fire neuron model: II. Inhomogeneous synaptic input and network properties, *Biol. Cybern.* **95**, 97 (2006).
- [16] N. Brunel, V. Hakim, and M. J. E. Richardson, Firing-rate resonance in a generalized integrate-and-fire neuron with sub-threshold resonance, *Phys. Rev. E* **67**, 051916 (2003).
- [17] N. Brunel, F. S. Chance, N. Fourcaud, and L. F. Abbott, Effects of Synaptic Noise and Filtering on the Frequency Response of Spiking Neurons, *Phys. Rev. Lett.* **86**, 2186 (2001).
- [18] J. W. Middleton, M. J. Chacron, B. Lindner, and A. Longtin, Firing statistics of a neuron model driven by long-range correlated noise, *Phys. Rev. E* **68**, 021920 (2003).
- [19] E. M. Izhikevich, Resonate-and-fire neurons, *Neural Netw.* **14**, 883 (2001).
- [20] M. J. E. Richardson, Spike-train spectra and network response functions for non-linear integrate-and-fire neurons, *Biol. Cybern.* **99**, 381 (2008).
- [21] L. A. da Silva and R. D. Vilela, Colored noise and memory effects on formal spiking neuron models, *Phys. Rev. E* **91**, 062702 (2015).
- [22] R. Mankin and S. Paekivi, Memory-induced resonancelike suppression of spike generation in a resonate-and-fire neuron model, *Phys. Rev. E* **97**, 012125 (2018).
- [23] T. Verechtchaguina, I. M. Sokolov, and L. Schimansky-Geier, First passage time densities in resonate-and-fire models, *Phys. Rev. E* **73**, 031108 (2006).
- [24] T. Schwalger, F. Droste, and B. Lindner, Statistical structure of neural spiking under non-Poissonian or other non-white stimulation, *J. Comput. Neurosci.* **39**, 29 (2015).
- [25] G. Uchida and M. Tanifuji, Transition rate dependence of interspike interval distributions of model neurons driven by two-state fluctuating input, *Phys. Rev. E* **98**, 032416 (2018).
- [26] F. Müller-Hansen, F. Droste, and B. Lindner, Statistics of a neuron model driven by asymmetric colored noise, *Phys. Rev. E* **91**, 022718 (2015).
- [27] E. Salinas and T. J. Sejnowski, Impact of correlated synaptic input on output firing rate and variability in simple neuronal models, *J. Neurosci.* **20**, 6193 (2000).
- [28] C. F. Stevens and A. M. Zador, Input synchrony and the irregular firing of cortical neurons, *Nat. Neurosci.* **1**, 210 (1998).
- [29] F. Droste and B. Lindner, Integrate-and-fire neurons driven by asymmetric dichotomous noise, *Biol. Cybern.* **108**, 825 (2014).
- [30] V. I. Klyatskin, *Lectures on Dynamics of Stochastic Systems* (Elsevier, London, 2011).
- [31] B. Lindner, Interspike interval statistics of neurons driven by colored noise, *Phys. Rev. E* **69**, 022901 (2004).
- [32] R. Mankin and N. Lumi, Statistics of a leaky integrate-and-fire model of neurons driven by dichotomous noise, *Phys. Rev. E* **93**, 052143 (2016).
- [33] R. Mankin and A. Rekker, Response to a periodic stimulus in a perfect integrate-and-fire neuron model driven by colored noise, *Phys. Rev. E* **94**, 062103 (2016).
- [34] A. D. Dorval, G. S. Russo, T. Hashimoto, W. Xu, W. M. Grill, and J. L. Vitek, Deep brain stimulation reduces neuronal entropy in the MPTP-primate model of Parkinson's disease, *J. Neurophysiology* **100**, 2807 (2008).
- [35] R. Sirovich, L. Sacerdote, and A. Villa, Cooperative behavior in a jump diffusion model for a simple network of spiking neurons, *Math. Biosci. Eng.* **11**, 385 (2014).
- [36] F. Wörgötter, E. Nelle, B. Li, and K. Funke, The influence of corticofugal feedback on the temporal structure of visual responses of cat thalamic relay cells, *J. Physiol.* **509**, 797 (1998).

- [37] A. Luczak, P. Barthó, S. L. Marguet, G. Buzsáki, and K. D. Harris, Sequential structure of neocortical spontaneous activity in vivo, *Proc. Natl. Acad. Sci. U.S.A.* **104**, 347 (2007).
- [38] S. R. Balind, Á. Magó, M. Ahmadi, N. Kis, Z. Varga-Nemeth, A. Lörincz, and J. K. Makara, Diverse synaptic and dendritic mechanisms of complex spike burst generation in hippocampal CA3 pyramidal cells, *Nat. Commun.* **10**, 1859 (2019).
- [39] B. N. Lundstrom, M. H. Higgs, W. J. Spain, and A. L. Fairhall, Fractional differentiation by neocortical pyramidal neurons, *Nat. Neurosci.* **11**, 1335 (2008).
- [40] S. Pækivi and R. Mankin, Bimodality of the interspike interval distributions for subordinated diffusion models of integrate-and-fire neurons, *Phys. A (Amsterdam)* **534**, 122106 (2019).
- [41] R. Mankin and A. Rekker, Effects of transient subordinators on the firing statistics of a neuron model driven by dichotomous noise, *Phys. Rev. E* **102**, 012103 (2020).
- [42] P. Lánský, Sources of periodical force in noisy integrate-and-fire models of neuronal dynamics, *Phys. Rev. E* **55**, 2040 (1997).
- [43] C. J. Wilson and Y. Kawaguchi, The origins of two-state spontaneous membrane potential fluctuations of neostriatal spiny neurons, *J. Neurosci.* **16**, 2397 (1996).
- [44] S. Eule and R. Friedrich, Subordinated Langevin equations for anomalous diffusion in external potentials – Biasing and decoupled external forces, *Europhys. Lett.* **86**, 30008 (2009).
- [45] A. Stanislavsky, K. Weron, and A. Weron, Anomalous diffusion with transient subordinators: A link to compound relaxation laws, *J. Chem. Phys.* **140**, 054113 (2014).
- [46] S. Orzel, W. Mydlarczyk, and A. Jurlewicz, Accelerating sub-diffusions governed by multiple-order time-fractional diffusion equations: Stochastic representation by a subordinated Brownian motion and computer simulations, *Phys. Rev. E* **87**, 032110 (2013).
- [47] T. Sandev, A. V. Chechkin, N. Korabel, H. Kantz, I. M. Sokolov, and R. Metzler, Distributed-order diffusion equations and multifractality: Models and solutions, *Phys. Rev. E* **92**, 042117 (2015).
- [48] T. Koren, J. Klafter, and M. Magdziarz, First passage times of Lévy flights coexisting with subdiffusion, *Phys. Rev. E* **76**, 031129 (2007).
- [49] K. Weron, A. Jurlewicz, M. Magdziarz, A. Weron, and J. Trzmiel, Overshooting and undershooting subordination scenario for fractional two-power-law relaxation responses, *Phys. Rev. E* **81**, 041123 (2010).
- [50] W. Teka, T. M. Marinov, and F. Santamaria, Neural spike timing adaptation described with a fractional leaky integrate-and-fire model, *PLDS Computat. Biol.* **10**, e1003526 (2014).
- [51] W. W. Teka, R. K. Upadhyay, and A. Mondal, Fractional-order leaky integrate-and-fire model with long-term memory and power law dynamics, *Neural Networks* **93**, 110 (2017).
- [52] B. I. Henry, T. A. M. Langlands, and S. L. Werne, Fractional Cable Models for Spiny Neuronal Dendrites, *Phys. Rev. Lett* **100**, 128103 (2008).
- [53] A. Stanislavsky, K. Weron, and A. Weron, Diffusion and relaxation controlled by tempered  $\alpha$ -stable processes, *Phys. Rev. E* **78**, 051106 (2008).
- [54] I. A. Ibragimov and K. E. Chernin, On the unimodality of stable laws, *Theory Probab. Appl.* **4**, 417 (1959).
- [55] D. R. Cox and P. A. W. Lewis, *The Statistical Analysis of Series of Events*, *Methuen's Monographs on Applied Probability and Statistics* (Methuen, London, 1996).
- [56] F. Farkhooi, M. F. Strube-Bloss, and M. P. Nawrot, Serial correlation in neural spike train: Experimental evidence, stochastic modeling, and single neuron variability, *Phys. Rev. E* **79**, 021905 (2009).
- [57] K. Rajdl and P. Lansky, Fano factor estimation, *Math. Biosci. Eng.* **11**, 105 (2014).
- [58] E. A. Stern, A. E. Kincaid, and C. J. Wilson, Spontaneous subthreshold membrane potential fluctuations and action potential variability of rat corticostriatal and striatal neurons in vivo, *J. Neurophysiol.* **77**, 1697 (1997).